Electronic Supplementary Information

Facile synthesis of naphthalene-based porous organic salts for photocatalytic oxidative coupling of amines in air

Shijie Wang[#], Juan Chen[#], Yanan Chang, Shuo Wang, Chaoran Meng, Zhouyang Long and Guojian Chen*

School of Chemistry and Materials Science, Jiangsu Key Laboratory of Green Synthetic Chemistry for Functional Materials, Jiangsu Normal University, Xuzhou, 221116, China.

*Corresponding author, E-mail: gjchen@jsnu.edu.cn.

[#]These authors contributed equally to this work.

Table S1 Synthesis of naphthalene-based porous organic salts under different conditions.

Entry	Samples	T (℃)	NDA concentration in DMF (mmol/mL)	NDSA concentration in DMF (mmol/mL)	t (h)	Yield (%)
1	NA-POS-1	80	0.1	0.1	12	60
2	NA-POS-1a	80	0.05	0.05	12	55
3	NA-POS-1b	80	0.15	0.15	12	59
4	NA-POS-1c	70	0.1	0.1	12	56
5	NA-POS-1d	90	0.1	0.1	12	61
6	NA-POS-1e	80	0.1	0.1	6	45
7	NA-POS-1f	80	0.1	0.1	24	65

Footnote: The typical naphthalene-based porous organic salt (NA-POS-1) was synthesized by a simple acid-base neutralization reaction between the mixture solution of 1,5-naphthalenediamine (NDA, 0.5 mmol) in 5 mL of DMF and 1,5-naphthalenedisulfonic acid (NDSA, 0.5 mmol) in 5 mL of DMF at 80 ℃ for 12 h. In order to understand the influence of the reaction temperature, reaction time and reactant concentration on the synthesis and crystallinity of NA-POS-1, other concentrations (0.05 and 0.15 mmol/mL for NDA and NDSA in 5 mL of DMF, respectively), temperatures (70 and 90 ℃) and time (6 and 24 h) were investigated to afford a series of porous organic salts NA-POS-1s (s=a~f). It is noted that the monomer NDA is hard to dissolve in the solvent DMF at room temperature but can be facilely dissolved in DMF at a high temperature exceeding 70 ℃, thus higher temperatures (70~90 ℃) are considered in the synthesis of NA-POS-1s. Under these different conditions, the solid yields of NA-POS-1s were ranging from 45%~65%. The low yield (45%) of NA-POS-1e should be due to a short reaction time of 6 h. The higher temperature and longer reaction time only slightly increased the yields (55%~65%) of NA-POS-1s, thus more optimized conditions was no longer investigated. By comparison, it was very suitable for the synthesis of NA-POS-1 with a considerable yield of 60% at 80 ℃ for 12 h (see Table S1, entry 1).

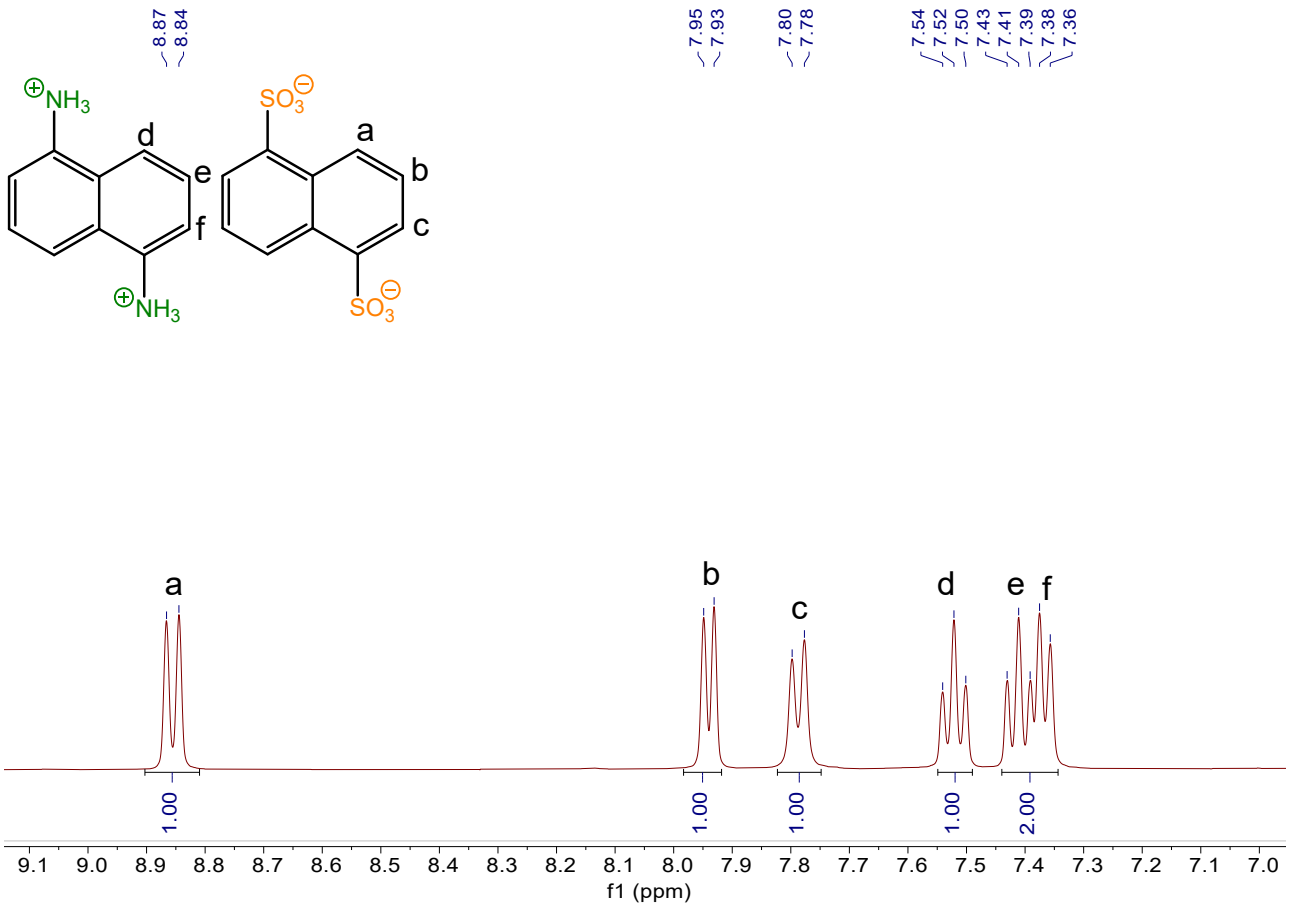

Fig. S1 ^{1}H NMR spectrum of NA-POS-1 dissolved in DMSO-d_6 at room temperature.

Table S2 The chemical structures of organic acid/base synthons, and surface areas of previously reported POSs.

Name	Organic acids	Organic bases	Surface area ($m^2 g^{-1}$)	Refs.
CPOS-1	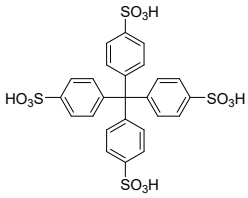	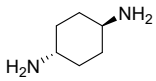	216 [a]	S1
CPOS-2	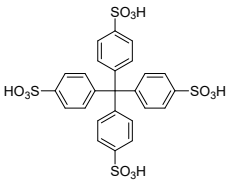	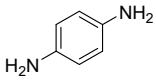	129 [a]	S1
CPOS-3	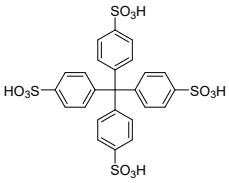	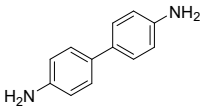	12 [a]	S1
CPOS-4	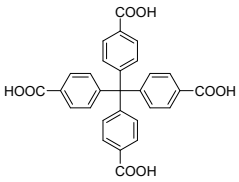	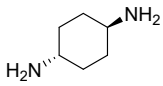	29 [a]	S1
CPOS-5	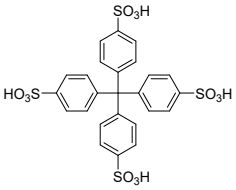	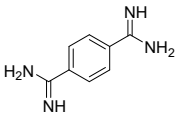	206 [a]	S2
CPOS-6	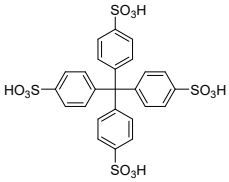	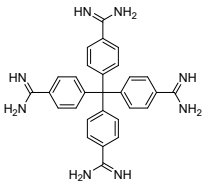	106.9 [a]	S3
d-POS-1	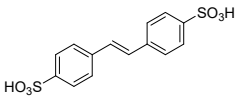	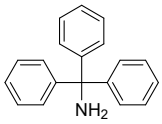	398 [b]	S4
Porous crystalline compound 1	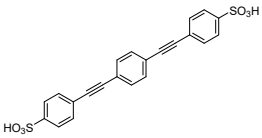	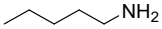	182 [b]	S5
HOF-GS-10	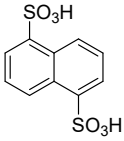	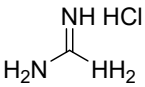	—	S6

TMPA/MTBPS	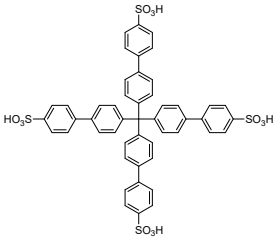	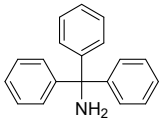	376 [b]/6.53 [c]	S7
TMPA-F/MTBPS	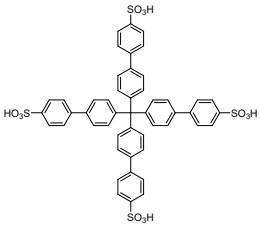	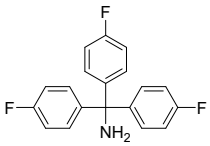	326 [b]/171 [c]	S7
TMPA-Cl/MTBPS	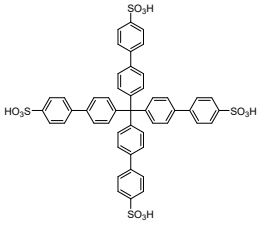	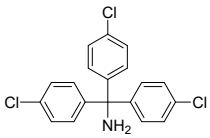	399 [b]/439 [c]	S7
TMPA-Br/MTBPS	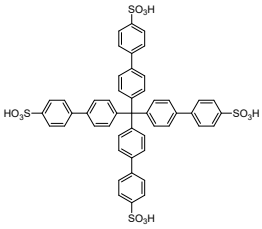	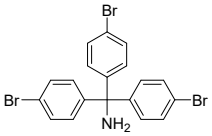	225 [b]/82.9 [c]	S7
F-2	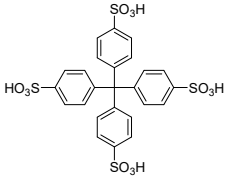	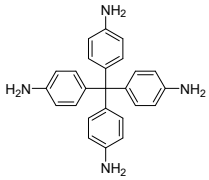	5.5 [c]	S8
F-3	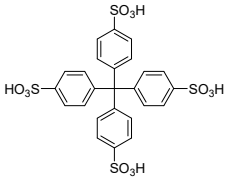	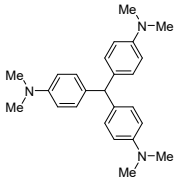	—	S8
NA-POS-1	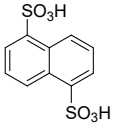	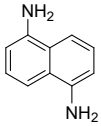	**61 [c]**	**This work**

[a] Calculated by the Dubinin-Astakhov method from CO_2 adsorption isotherms at 273 K; [b] Calculated by the Brunauer-Emmett-Teller (BET) method from CO_2 adsorption isotherms at 195 K. [c] Calculated by the Brunauer-Emmett-Teller (BET) method from N_2 adsorption isotherms at 77 K.

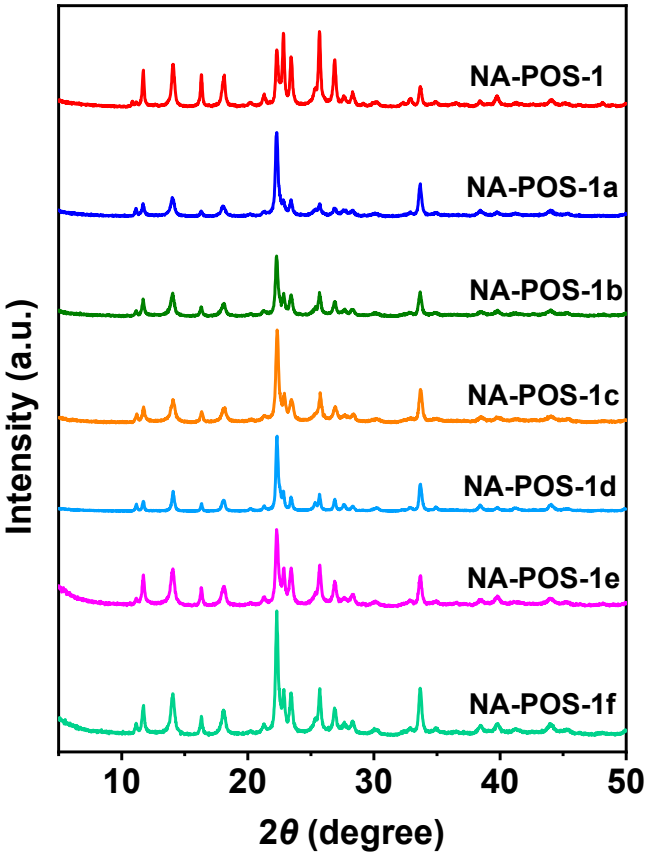

Fig. S2 XRD patterns of NA-POS-1 and NA-POS-1s (s=a~f).

As shown in Fig. S2, the XRD patterns of NA-POS-1 and NA-POS-1s (s=a~f) show that all these POSs display a set of strong Bragg diffraction peaks at the same positions (2θ=11.7°, 14.1°, 16.3°, 18.0°, 22.3°, 22.9°, 25.6°, 26.9° and 33.6°), indicative of their similar highly crystalline structures. However, the peak intensities at the above positions have some differences, indicating their different crystallinity of NA-POS-1s that prepared under different synthetic conditions including the reaction temperature, reaction time and reactant concentration (Table S1). As a result, a relatively higher crystallinity of NA-POS-1 can be obtained with a suitable concentration (0.1 mmol/mL) of NDA and NSDA in DMF at 80 ℃ for 12 h (see Table S1, entry 1).

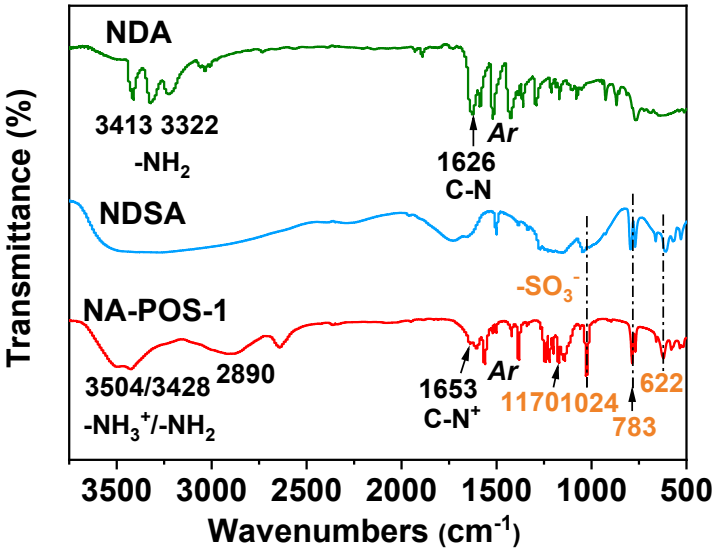

Fig. S3 FTIR spectra of NDA, NDSA and NA-POS-1.

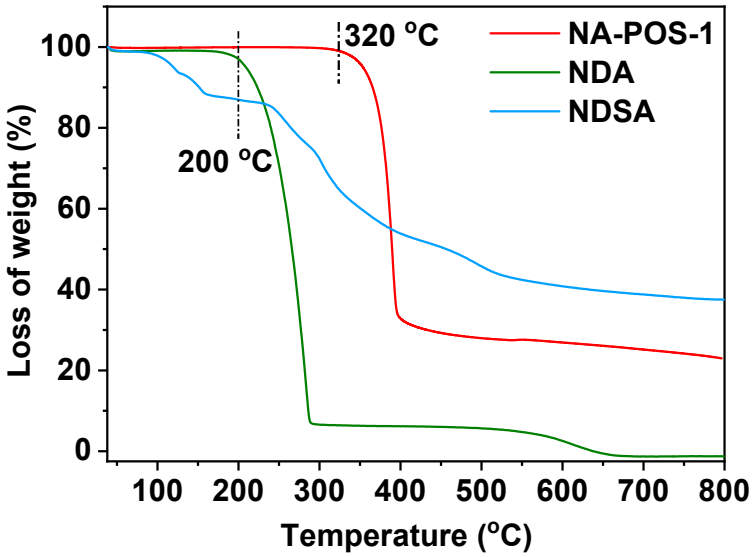

Fig. S4 The thermogravimetric analysis (TGA) curves of NA-POS-1, NDA and NDSA under N_2 atmosphere.

As shown in Fig. S4, both the naphthalene monomers NDA and NDSA have poor thermal stability only to 200 °C under N_2 atmosphere, while the formed polymeric organic salt NA-POS-1 exhibits excellent thermal stability to 320 °C and good moisture resistance. Therefore, the self-assembly of NDA and NDSA into the porous organic salt NA-POS-1 by both ionic and hydrogen bonding interactions can significantly enhance the thermal stability and moisture resistance ability of NA-POS-1.

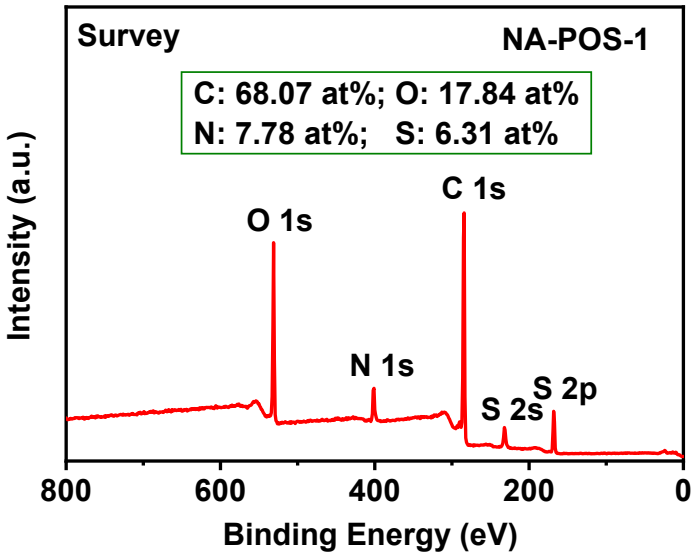

Fig. S5 XPS survey spectra of NA-POS-1 with the elemental compositions with atomic concentrations of C (68.07 at %), O (17.84 at %), N (7.78 at %) and S (6.31 at %).

Table S3 Visible-light-driven photocatalytic oxidative coupling of benzylamine in air using NA-POS-1 and NA-POS-1s (s=a~f) as photocatalysts.[a]

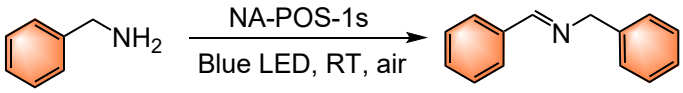

Entry	Catalyst	Conversion (%)	Selectivity (%)
1	NA-POS-1	99	99
2	NA-POS-1a	93	99
3	NA-POS-1b	99	98
4	NA-POS-1c	95	99
5	NA-POS-1d	99	96
6	NA-POS-1e	72	99
7	NA-POS-1f	99	98

[a] Reaction conditions: benzylamine (0.5 mmol), catalyst (5 mg), blue LEDs lamp (5 W), solvent-free, room temperature (RT), in ambient air (1 atm), 6 h.

The screening experiments of NA-POS-1 and NA-POS-1s catalysts were carried out in the visible-light-driven photocatalytic oxidative coupling of benzylamine with O_2 from ambient air irradiated by blue LEDs (Table S3). The desired heterogeneous photocatalyst NA-POS-1 afforded a perfect conversion of 99% and selectivity of 99% for the product (Table S3, entry 1), while the control catalysts NA-POS-1b, NA-POS-1d and NA-POS-1f also provided a high conversion of 99% and slight decrease selectivity of 96%~98%. Besides, the catalysts NA-POS-1a and NA-POS-1c that prepared at a low reactant concentration (0.05 mmol/mL) and a low temperature (70 °C) gave slight decrease conversions of 93% and 95% compared with 99%, only the catalyst NA-POS-1e that prepared in a short time (6 h) gave a relatively low conversion of 72%. In fact, these catalysts NA-POS-1 and NA-POS-1s have similar crystalline structures but with different degrees of crystallinity. In particular, the good crystallinity of NA-POS-1e did not give the desired catalytic activity, indicating the high crystallinity of NA-POS-1 has certain a favorable influence on the photocatalytic performance, but may be not the most critical factor. Generally, a longer reaction time and higher temperature are beneficial to obtain highly crystalline and cross-linked NA-POS-1 with extended π-conjugated systems and charged ionic units for cooperatively enhancing the photocatalytic activity.

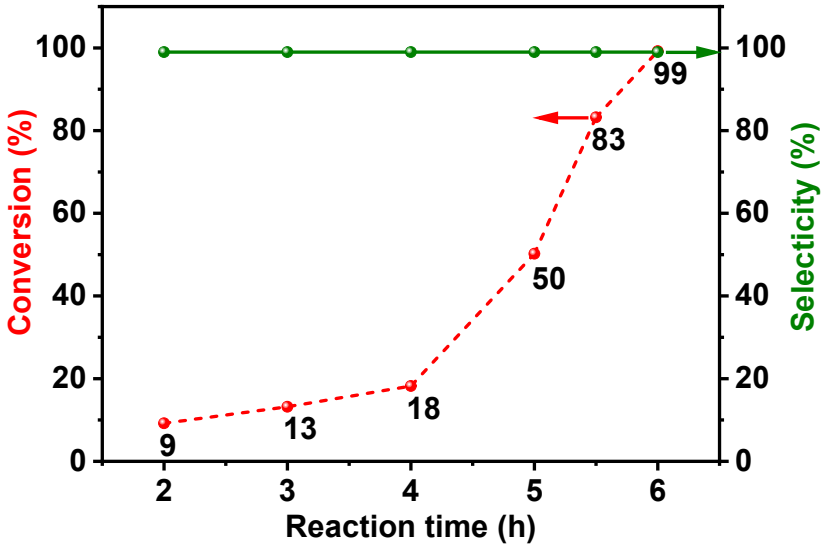

Fig. S6 The kinetic curve in showing the reaction time course of NA-POS-1 for the photocatalytic oxidative coupling of benzylamine in air. Reaction conditions: benzylamine (0.5 mmol), the catalyst NA-POS-1 (5 mg), solvent-free, blue LEDs (5 W), room temperature, in air, 2~6 h.

As shown in Fig. S6, the kinetic curve of NA-POS-1 with respect to the reaction time (2~6 h) was carried out in the photocatalytic oxidative coupling of benzylamine in air. At the initial period of time (0~4 h), the conversion of benzylamine slowly increased to 18%, indicating the existence of the induction period in the initial stage of this photocatalytic reaction over the catalyst NA-POS-1. At the time course of 4~6 h, the conversion rapidly increased from 18% to 99%, which could be attributed to the fast reaction kinetics behavior at this time period. In particular, the conversion dramatically increased from 50% to 99% at the time course of 5~6 h, and a high conversion of 83% was also obtained at 5.5 h, confirming the fast reaction kinetics behavior in a very short time after the induction period for this reaction over the catalyst NA-POS-1.

Table S4 Comparisons for photocatalytic performance of the photocatalytic oxidative of benzylamine with O_2 or air at room temperature (RT) over metal-free porous organic polymer photocatalysts.

Entry	Photocatalyst	Reaction conditions	Conversion (%)	Refs.
1	B-BO-1,3,5	Benzylamine (1 mmol), Cat. (6 mg), fluorescent light (25 W), CH_3CN (3 mL), RT, O_2, 24 h	99	S9
2	AN-POP	Benzylamine (0.5 mmol), Cat. (0.5% mmol), blue LEDs (24 W), CH_3CN (5 mL), RT, air, 24 h	95	S10
3	JUM12	Benzylamine (0.5 mmol), Cat. (1% mmol), green LEDs (12 W), CH_3CN (4 mL), RT, air, 24 h	97	S11
4	PAA-CMP	Benzylamine (0.5 mmol), Cat. (15 mg), white LEDs, CH_3CN (10 mL), RT, O_2, 16 h	86	S12
5	JNU-211	Benzylamine (0.4 mmol), Cat. (4 mg), blue LEDs, CH_3CN (4 mL), RT, air, 12 h	99	S13
6	VCR-POP-1	Benzylamine (0.4 mmol), Cat. (3 mg), white LEDs (5 W), CH_3CN (2 mL), RT, air, 12 h	97	S14
7	C-CMP	Benzylamine (1 mmol), Cat. (20 mg), Xe lamp (150 W), CH_3CN (2 mL), RT, O_2, 4 h	99	S15
8	TA-Por-sp^2 -COF	Benzylamine (1 mmol), Cat. (5 mg), white LEDs (15 W), CH_3CN (20 mL), RT, air, 2 h	99.9	S16
9	DCM-HCPs	Benzylamine (0.2 mmol), Cat. (10 mg), LED lamp (455 nm, 50 W), CH_3CN (10 mL), RT, air, 1.5 h	99.8	S17
10	TA-sp^2c-COF	Benzylamine (0.3 mmol), Cat. (5 mg), blue LEDs, CH_3CN (1 mL), RT, O_2, 1.2 h	90	S18
11	TFPT-BMTH	Benzylamine (0.2mmol), Cat. (5 mmol%), blue LEDs (30 W), H_2O (5 mL), RT, air atmosphere, 24 h	99	S19
12	TFB-33-DMTH	Benzylamine (0.2 mmol), Cat. (10 mg), blue LEDs (30 W), H_2O (2 mL), RT, air atmosphere, 20 h	99	S20
13	PTZ-TTA-COF	Benzylamine (0.1 mmol), Cat. (2 mg), blue LEDs (12 W), CD_3CN (1 mL), RT, air, 1 h	92	S21

14	PTA-TTA-COF	Benzylamine (0.1 mmol), Cat. (2 mg), natural sunlight, CD_3CN (1 mL), in open air at room temperature, 3 h	71	S21
15	PAA-CMP	Benzylamine (2 g), Cat. (100 mg), natural sunlight, CH_3CN (100 mL), 28~35 °C, 48 h	65	S22
16	TPT-porp	Benzylamine (0.1 mmol), Cat. (5 mg), natural sunlight, CH_3CN (3 mL), air, 6 h	65	S23
17	**NA-POS-1**	**Benzylamine (0.5 mmol), Cat. (5 mg), blue LEDs (5 W), solvent-free, RT, air, 6 h**	**99**	**This work**

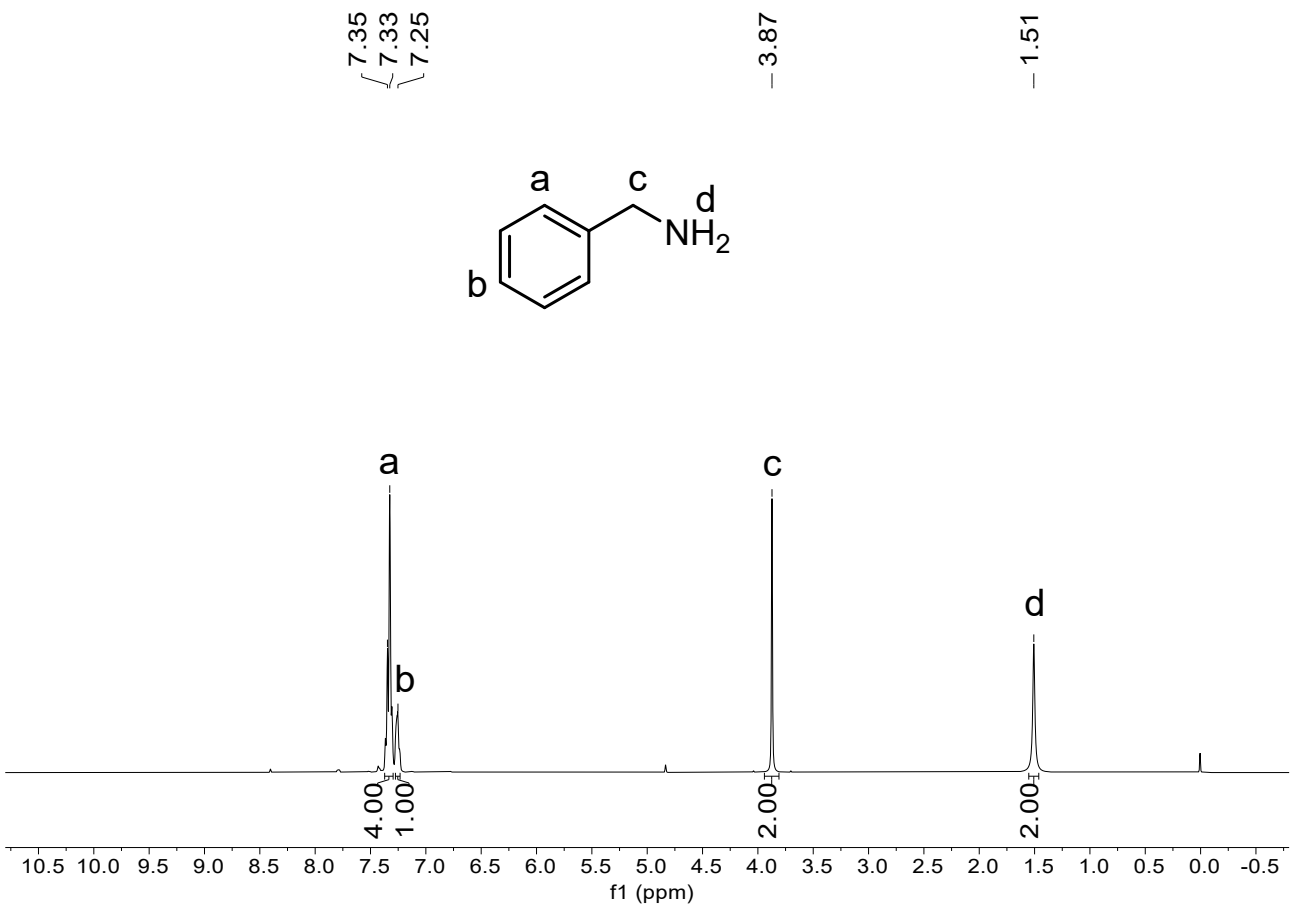

Fig. S7 ^{1}H NMR spectrum of benzylamine after the solubility test of the catalyst NA-POS-1.

In a typical run, a suitable amount of the catalyst NA-POS-1 and the reaction substrate benzylamine were magnetically stirred in dark at room temperature for 6 h under atmospheric air. After the filtration, the mass of the catalyst NA-POS-1 has no obvious loss and the liquid benzylamine was determined by the ^{1}H NMR in the solvent $CDCl_3$. By analyzing the ^{1}H NMR (Fig. S7), the solution involved the substrate benzylamine without any molecular components of the catalyst NA-POS-1 (see Fig. S1), indicating the insolubility of NA-POS-1 in the benzylamine. When the reaction system was radiated the light of blue LEDs, the photocatalytic conversion of benzylamine into the product *(E)*-N-benzyl-1-phenylmethanimine (**2a**) was effectively achieved over the catalyst NA-POS-1. After such a photocatalytic reaction, the ^{1}H NMR spectrum (Fig. S8) showed that the mixture solution mainly involved the product **2a** without any components of NA-POS-1, also indicating no leaching of the catalyst NA-POS-1 into the solution after the reaction. The above experimental results demonstrated that the catalyst NA-POS-1 was insoluble in the reaction system before and after the reaction, and thus was a true heterogeneous catalyst in such a solvent-free photocatalytic reaction.

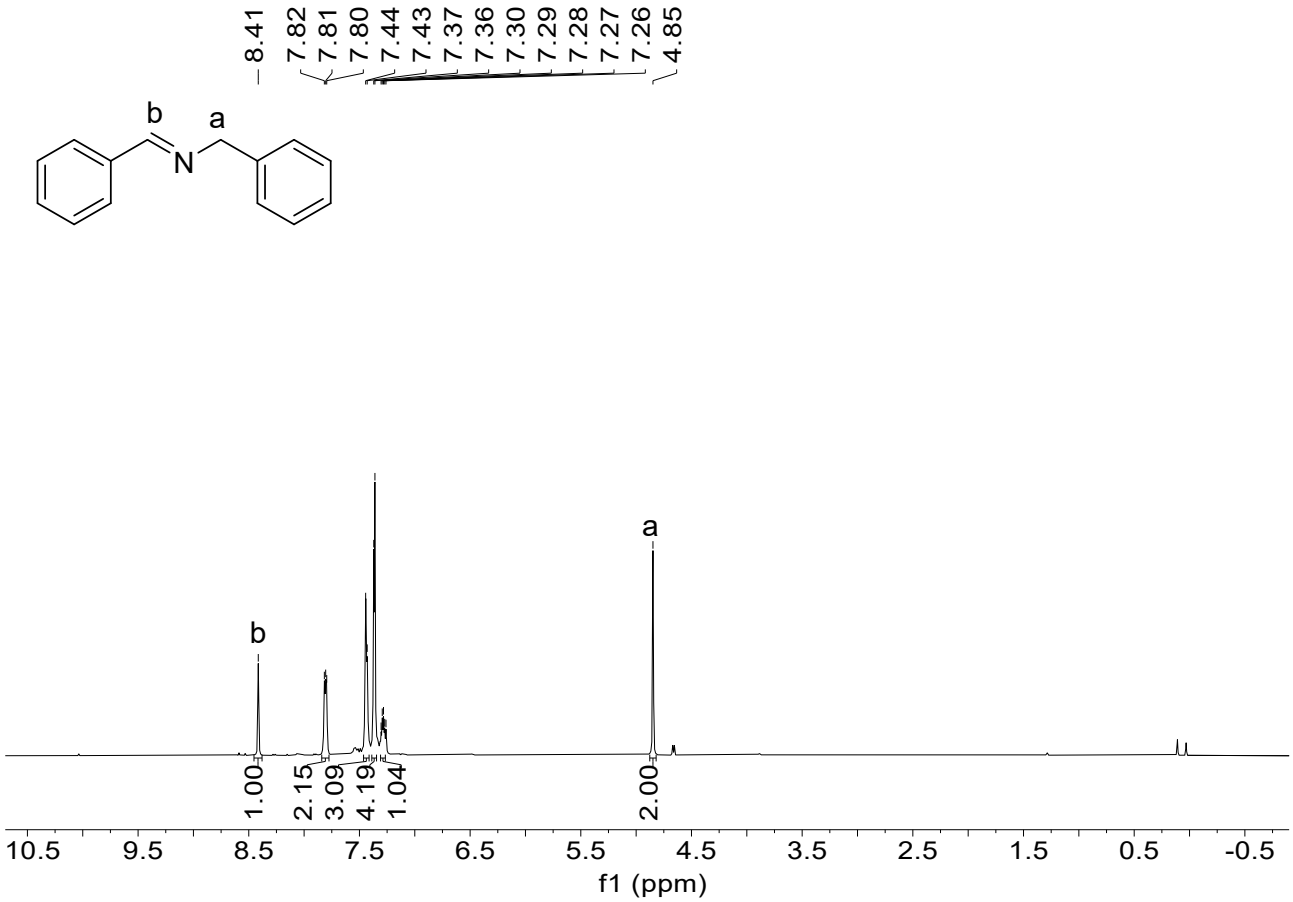

Fig. S8 ^{1}H NMR spectrum of *(E)*-N-benzyl-1-phenylmethanimine (**2a**) (400 MHz, $CDCl_3$): δ=8.41 (s, 1H), 7.82~7.80 (m, 2H), 7.44~7.26 (m, 8H) and 4.85 ppm (s, 2H). Reaction conditions: blue LEDs (5 W), room temperature, in air, 6 h, conversion of 99%, selectivity of 99%.

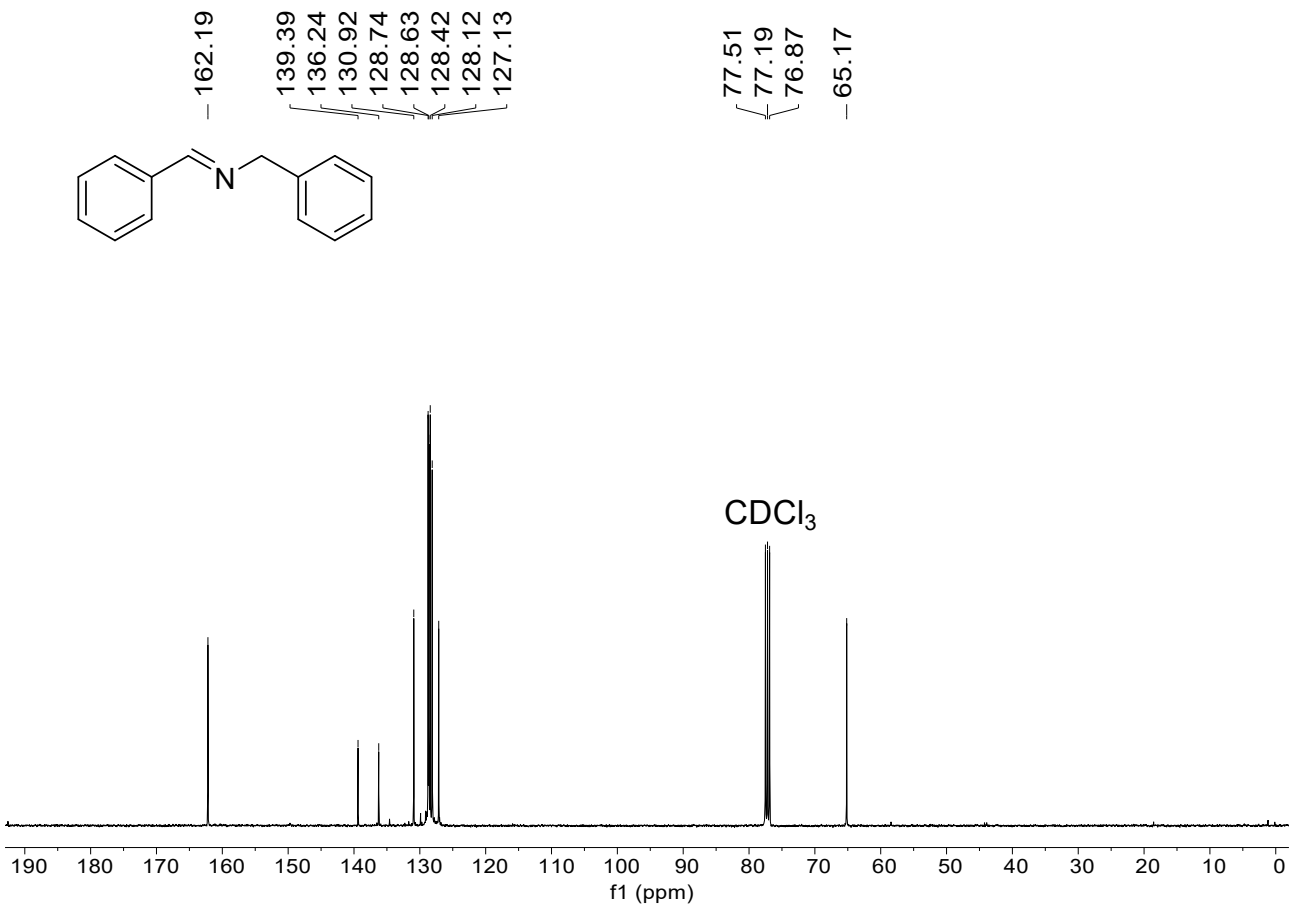

Fig. S9 ^{13}C NMR spectrum of *(E)*-N-benzyl-1-phenylmethanimine (**2a**) (100 MHz, $CDCl_3$): δ=162.19, 139.39, 136.24, 130.92, 128.74, 128.63, 128.42, 128.12, 127.13 and 65.17 ppm.

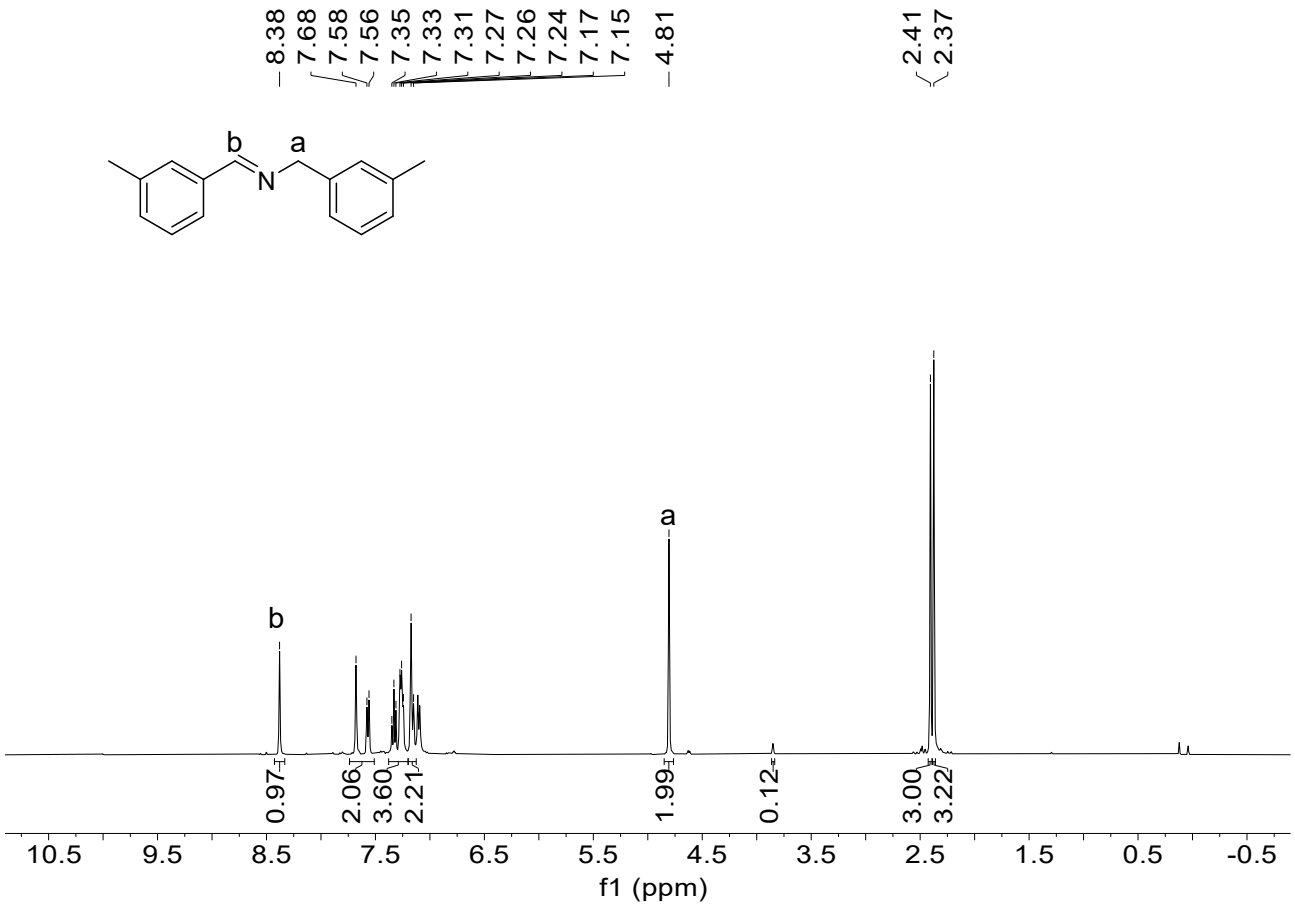

Fig. S10 ^{1}H NMR spectrum of *(E)*-N-(3-methylbenzyl)-1-(3-methylbenzyl)methanimine (**2b**) (400 MHz, $CDCl_3$): δ=8.38 (s, 1H), 7.68~7.58 (d, 2H), 7.35~7.24 (dt, 4H), 7.17~7.15 (d, 2H), 4.81 (s, 2H), 2.41 (s, 3H) and 2.37 ppm (s, 3H). Reaction conditions: blue LEDs (5 W), room temperature, in air, 8 h, conversion of 94%, selectivity of 99%.

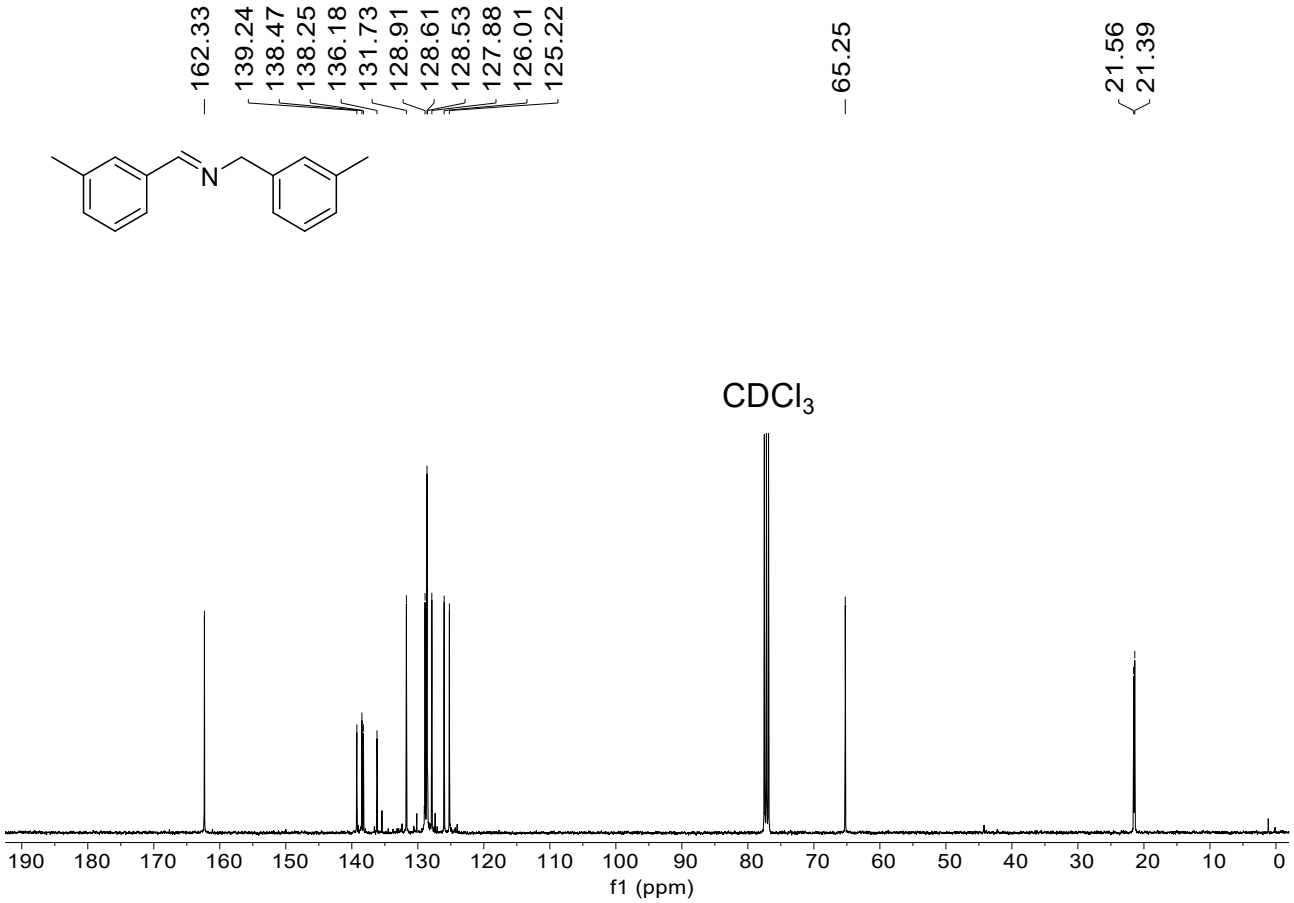

Fig. S11 ^{13}C NMR spectrum of *(E)*-N-(3-methylbenzyl)-1-(3-methylbenzyl)methanimine (**2b**) (100 MHz, $CDCl_3$): δ=162.33, 139.24, 138.47, 138.25, 136.18, 131.73, 128.91, 128.61, 128.53, 127.88, 126.01, 125.22, 65.25, 21.56 and 21.39 ppm

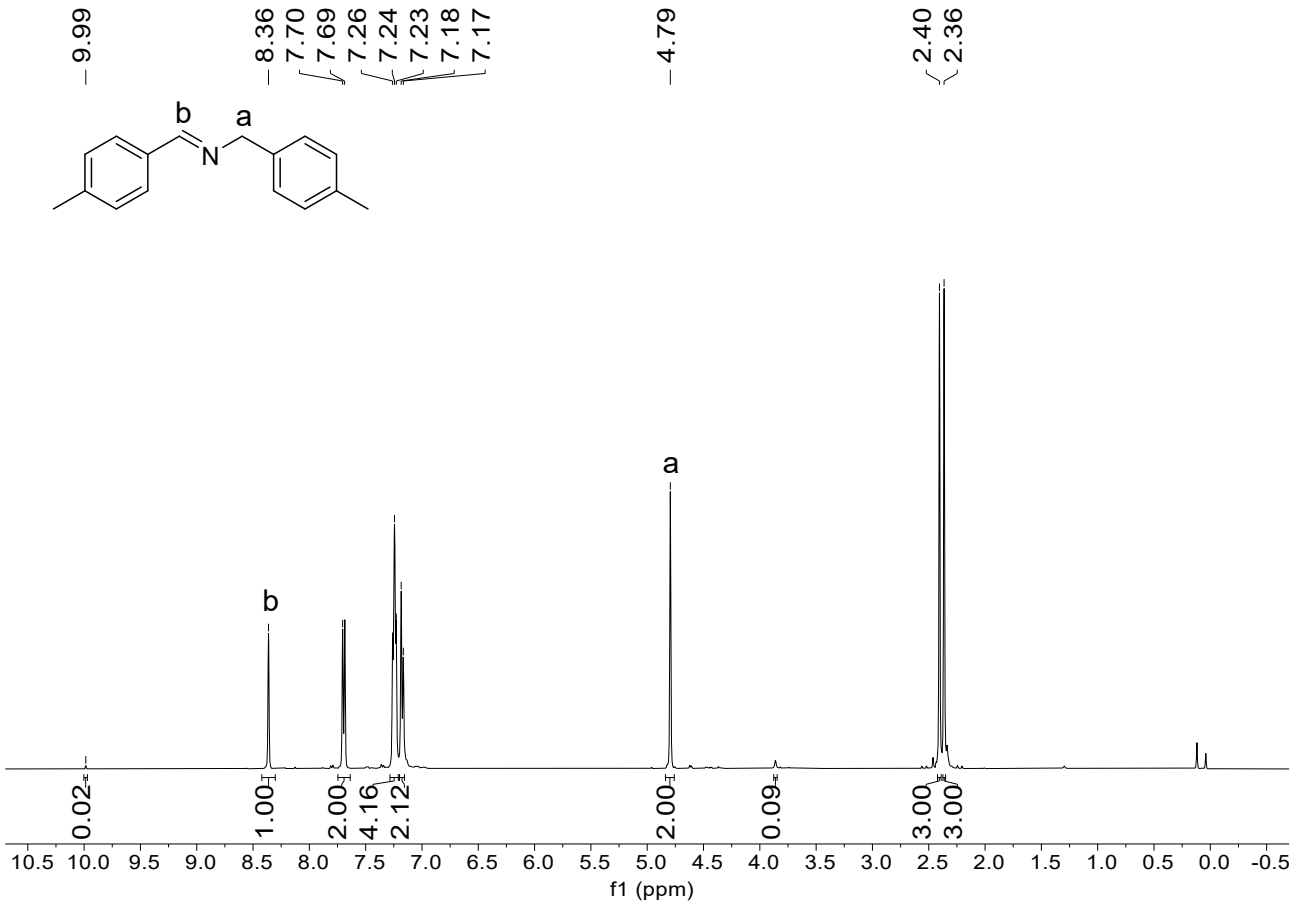

Fig. S12 ^{1}H NMR spectrum of *(E)*-N-(4-methylbenzyl)-1-(4-methylbenzyl)methanimine (**2c**) (400 MHz, $CDCl_3$): δ=8.36 (s, 1H), 7.70~7.69 (d, 2H), 7.26~7.23 (dd, 4H), 7.18~7.17 (d, 2H), 4.79 (s, 2H), 2.40 (s, 3H) and 2.36 ppm (s, 3H). Reaction conditions: blue LEDs (5 W), room temperature, in air, 7 h, conversion of 96%, selectivity of 99%.

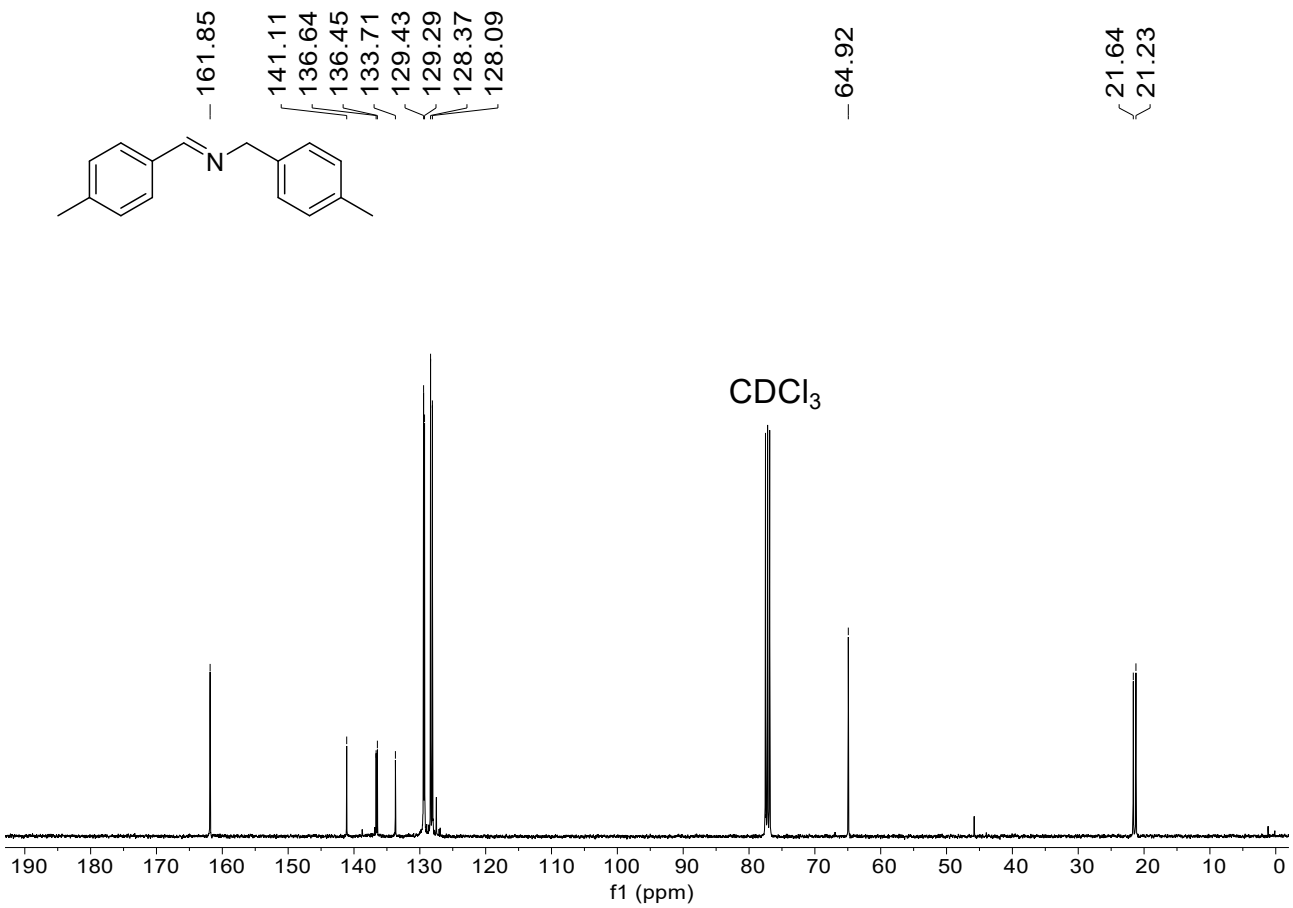

Fig. S13 ^{13}C NMR spectrum of *(E)*-N-(4-methylbenzyl)-1-(4-methylbenzyl)methanimine (**2c**) (100 MHz, $CDCl_3$): δ=161.85, 141.11, 136.64, 136.45, 133.71, 129.43, 129.29, 128.37, 128.09, 64.92, 21.64 and 21.23 ppm.

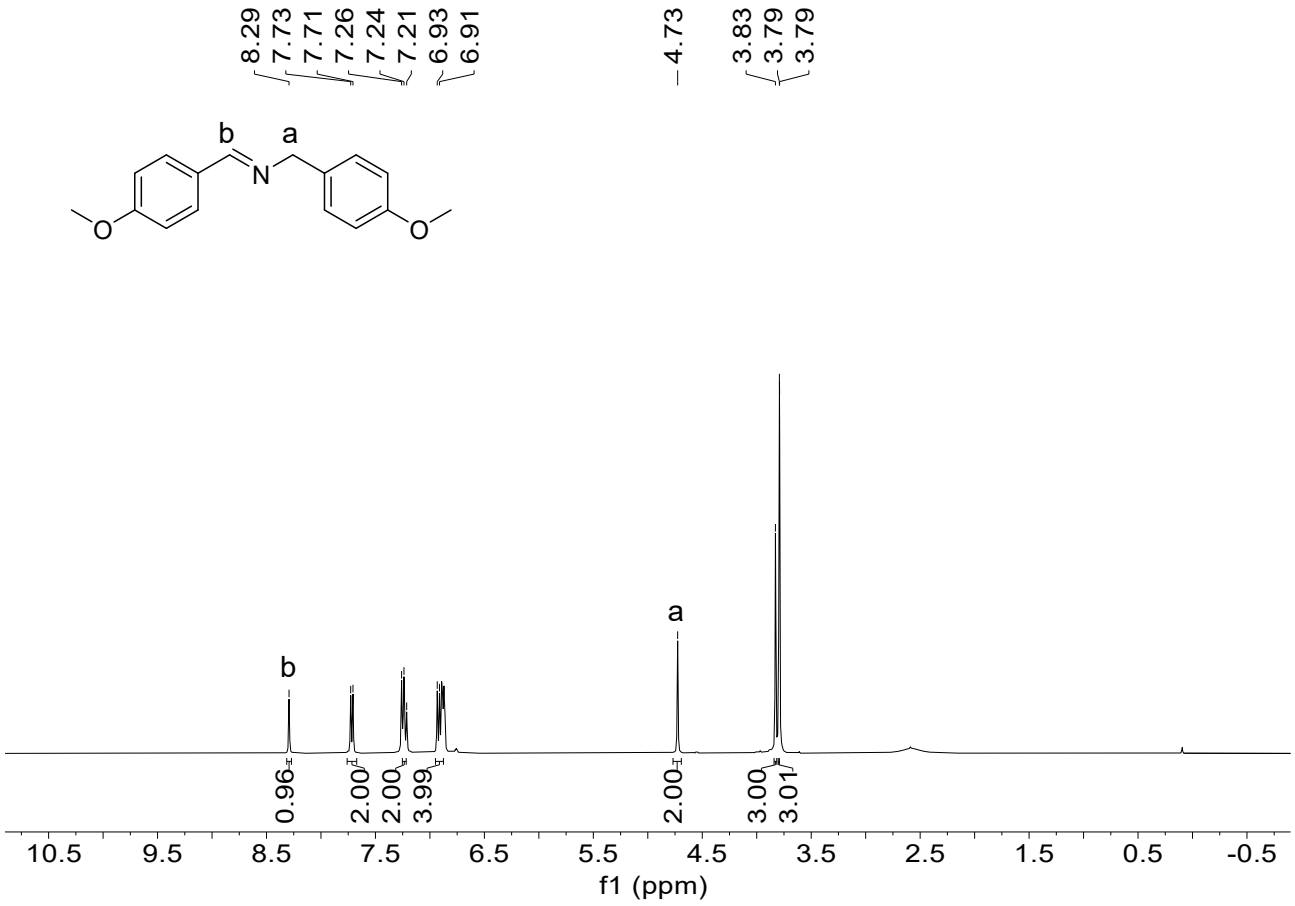

Fig. S14 ^{1}H NMR spectrum of *(E)*-N-(4-methoxybenzyl)-1-(4-methoxyphenyl)methanimine (**2d**) (400 MHz, $CDCl_3$): δ=8.29 (s, 1H), 7.73~7.71 (d, 2H), 7.24~7.21 (d, 2H), 6.93~6.91 (dd, 4H), 4.73 (s, 2H), 3.83 (s, 3H) and 3.79 ppm (s, 3H). Reaction conditions: blue LEDs (5 W), room temperature, in air, 8 h, conversion of 99%, selectivity of 99%.

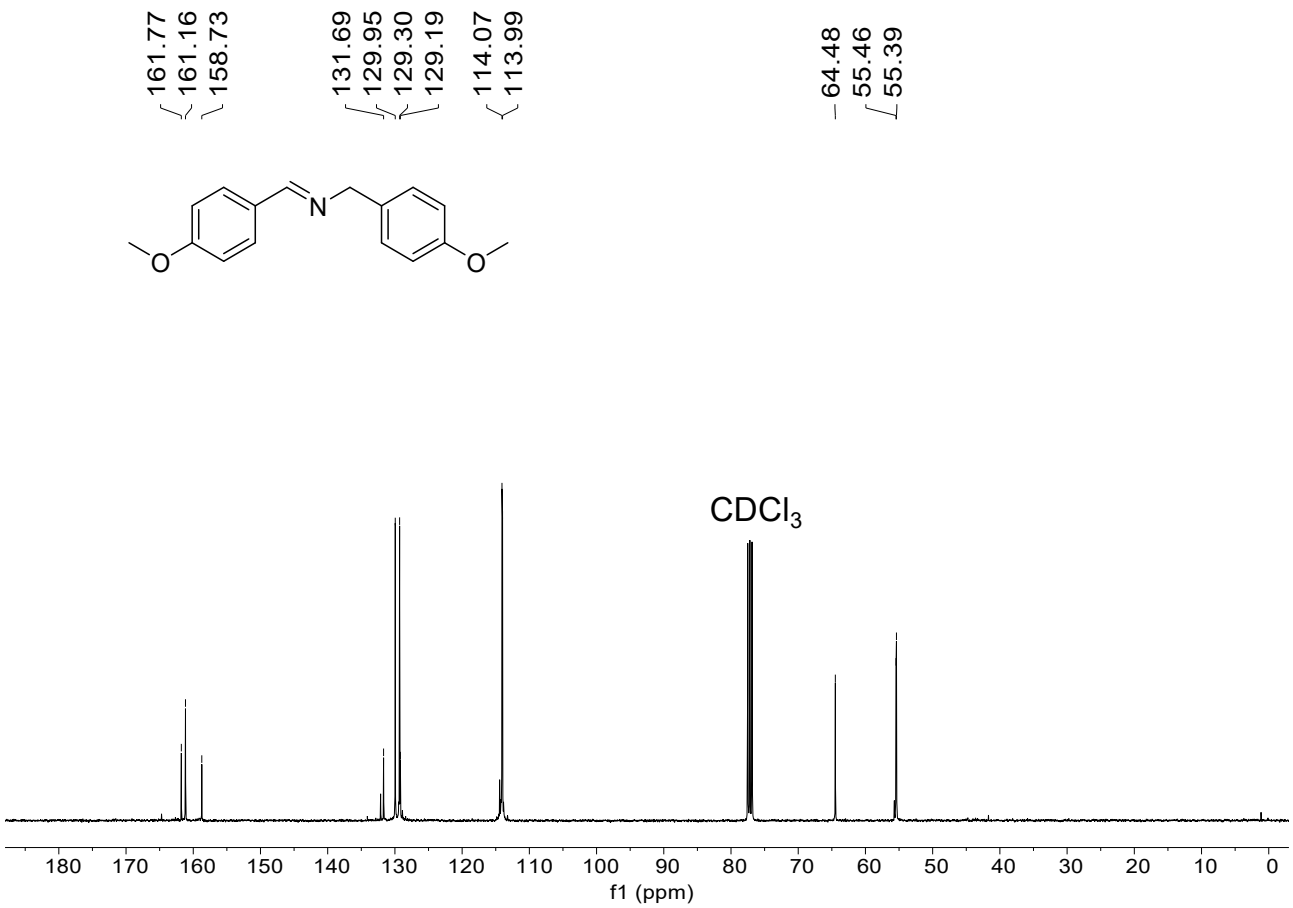

Fig. S15 ^{13}C NMR spectrum of *(E)*-N-(4-methoxybenzyl)-1-(4-methoxyphenyl)methanimine (**2d**) (100 MHz, $CDCl_3$): δ=161.77, 161.16, 158.73, 131.69, 129.95, 129.30, 129.19, 114.07, 113.99, 64.48, 55.46 and 55.39 ppm.

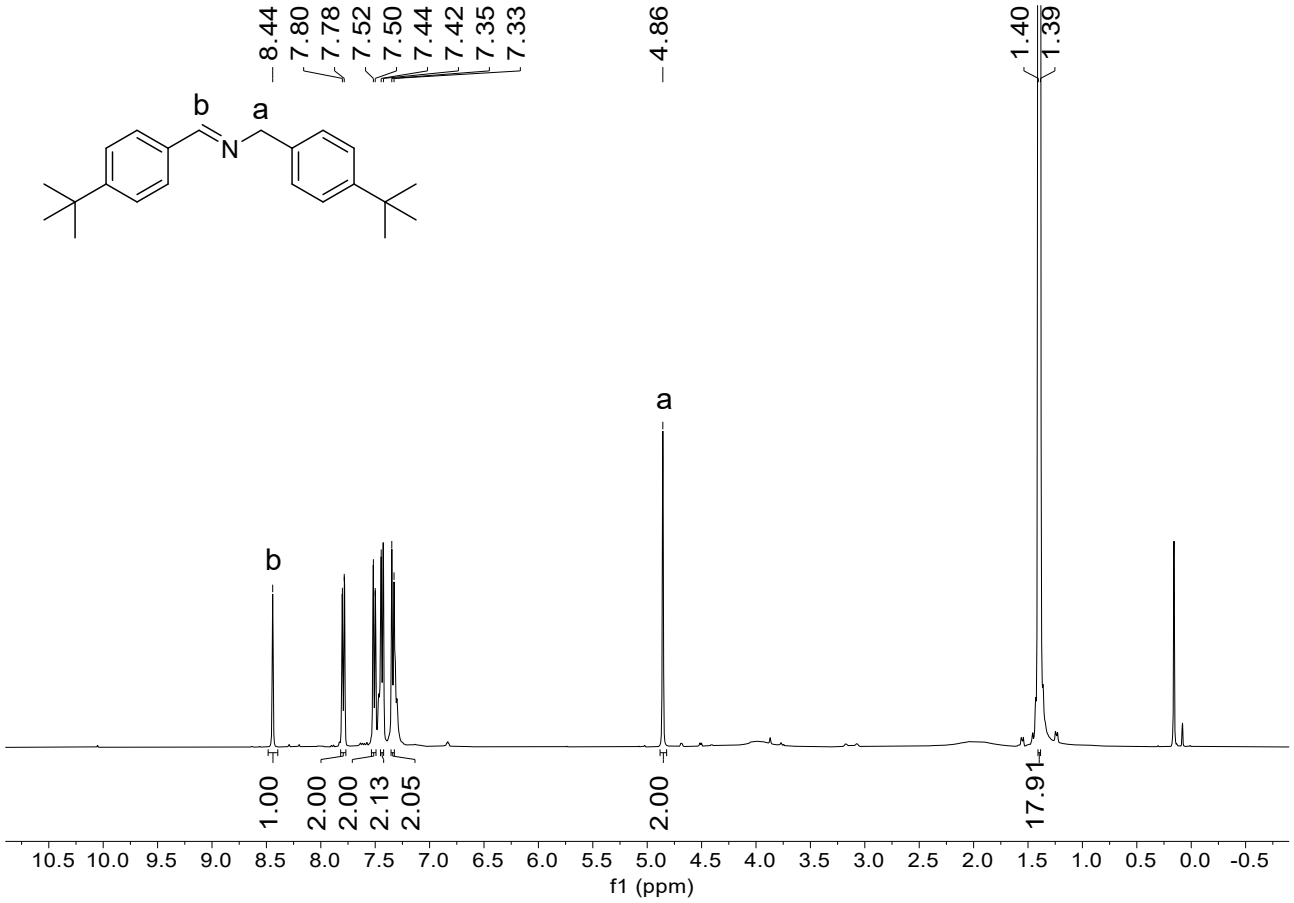

Fig. S16 ^{1}H NMR spectrum of *(E)*-N-(4-(tert-butyl)benzyl)-1-(4-(tert-butyl)phenyl)methanimine **(2e)** (400 MHz, $CDCl_3$): δ=8.44 (s, 1H), 7.80~7.78 (d, 2H), 7.52~7.50 (d, 2H), 7.44~7.42 (d, 2H), 7.35~7.33 (d, 2H), 4.86 (s, 2H) and 1.40~1.39 ppm (d, 18H). Reaction conditions: blue LEDs (5 W), room temperature, in air, 10 h, conversion of 99%, selectivity of 99%.

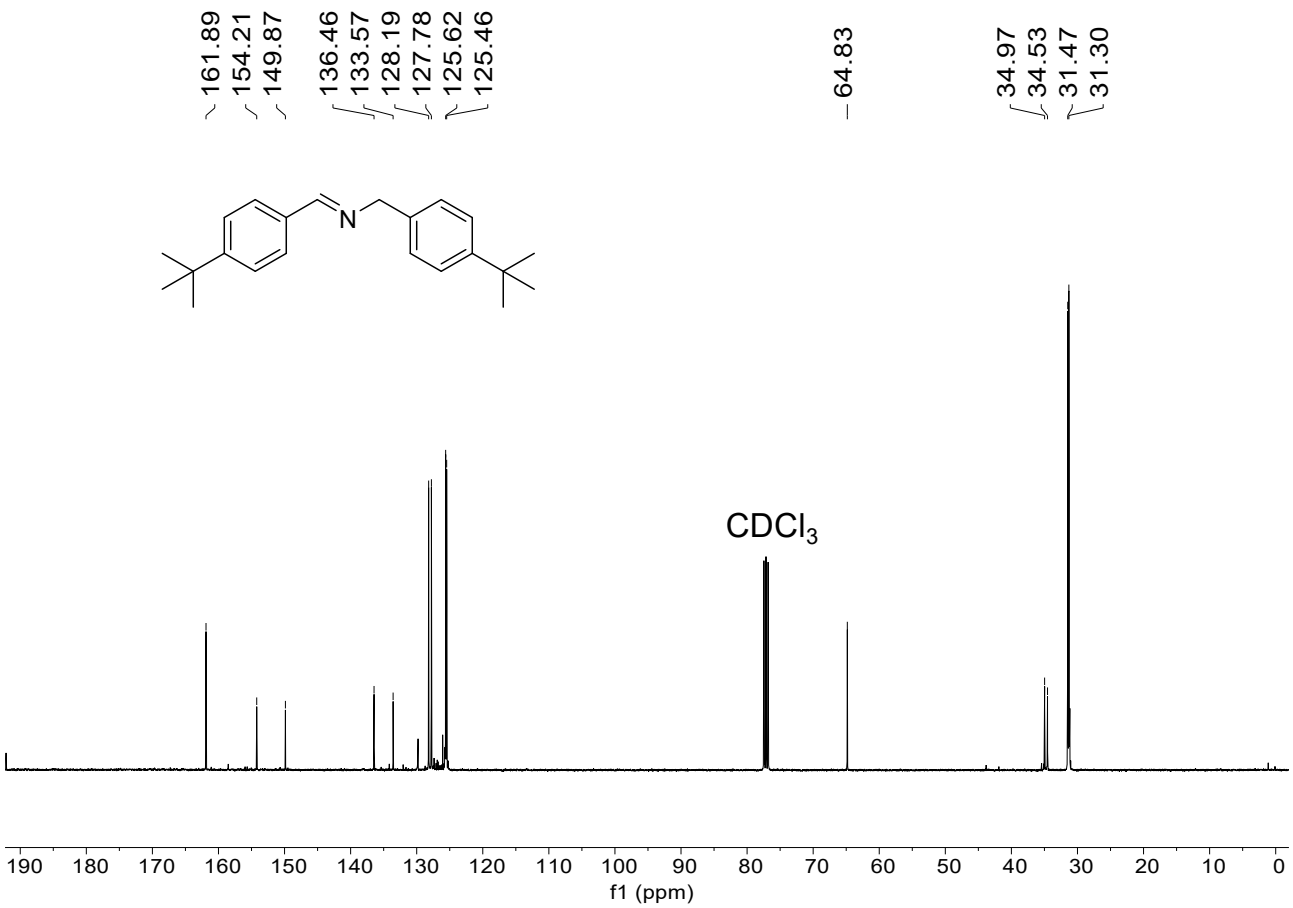

Fig. S17 ^{13}C NMR spectrum of *(E)*-N-(4-(tert-butyl)benzyl)-1-(4-(tert-butyl)phenyl)methanimine (**2e**) (100 MHz, $CDCl_3$): δ=161.89, 154.21, 149.87, 136.46, 133.57, 128.19, 127.78, 125.62, 125.46, 64.83, 34.97, 34.53, 31.47 and 31.30 ppm.

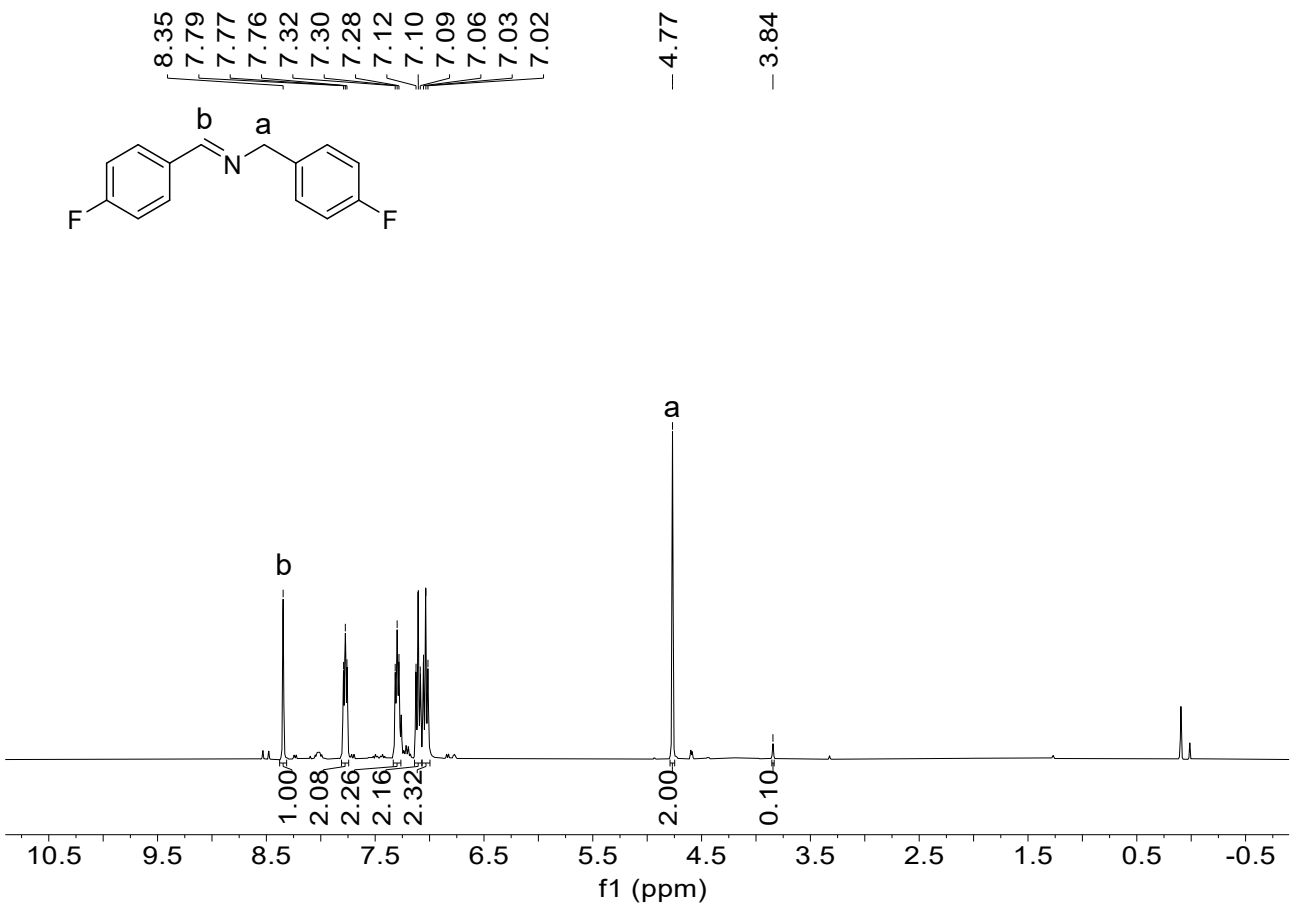

Fig. S18 ^{1}H NMR spectrum of *(E)*-N-(4-fluorobenzyl)-1-(4-fluorophenyl)methanimine (**2f**) (400 MHz, $CDCl_3$): δ=8.35 (s, 1H), 7.79~7.76 (m, 2H), 7.32~7.28 (m, 2H),7.12~7.09 (m, 2H), 7.06~7.02 (m, 2H) and 4.77 ppm (s, 2H). Reaction conditions: blue LEDs (5 W), room temperature, in air, 10 h, conversion of 95%, selectivity of 99%.

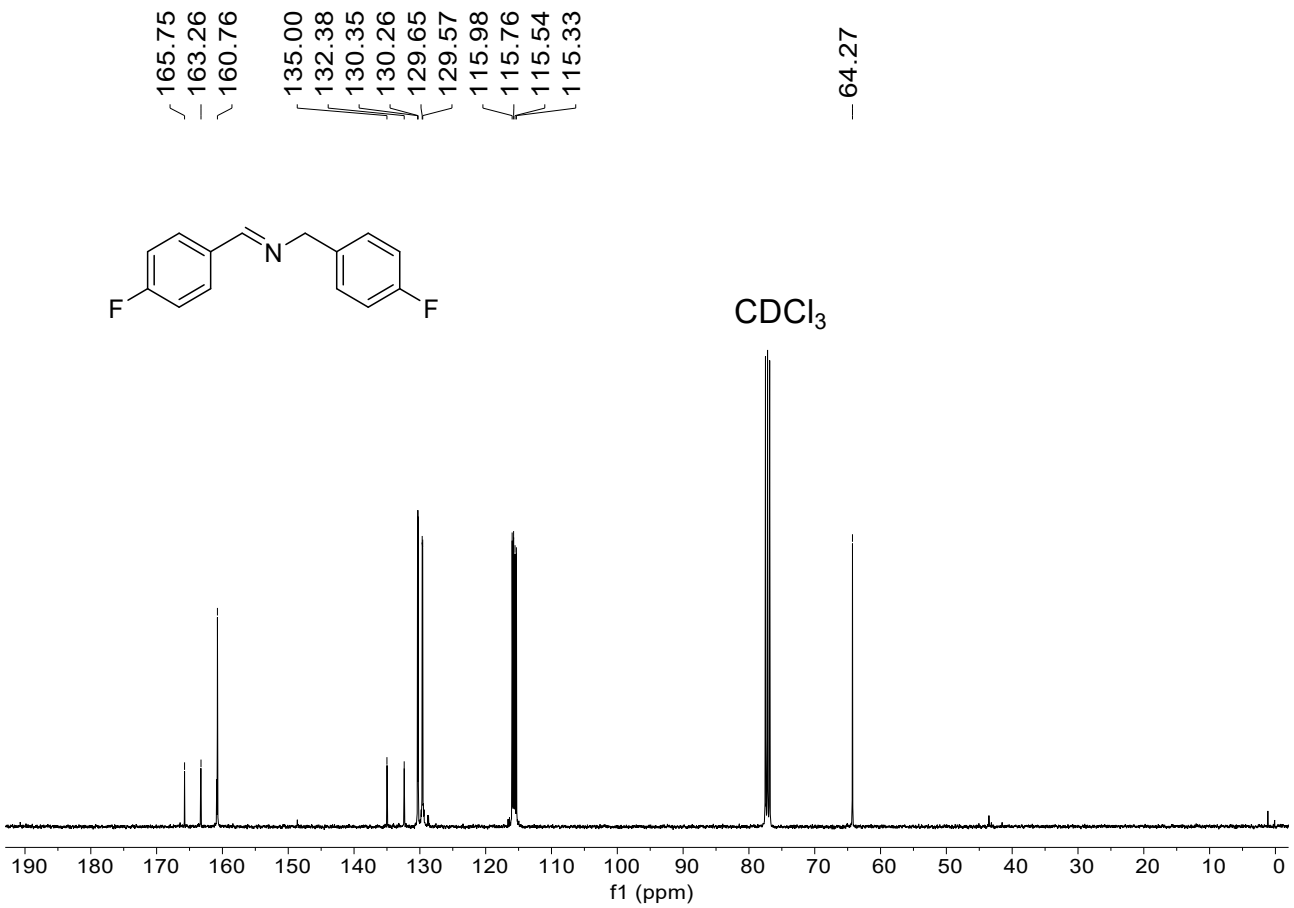

Fig. S19 ^{13}C NMR spectrum of *(E)*-N-(4-fluorobenzyl)-1-(4-fluorophenyl)methanimine (**2f**) (100 MHz, $CDCl_3$): δ=165.75, 163.26, 160.76, 135.00, 132.38, 130.35, 130.26, 129.65, 129.57, 115.98, 115.76, 115.54, 115.33 and 64.27 ppm.

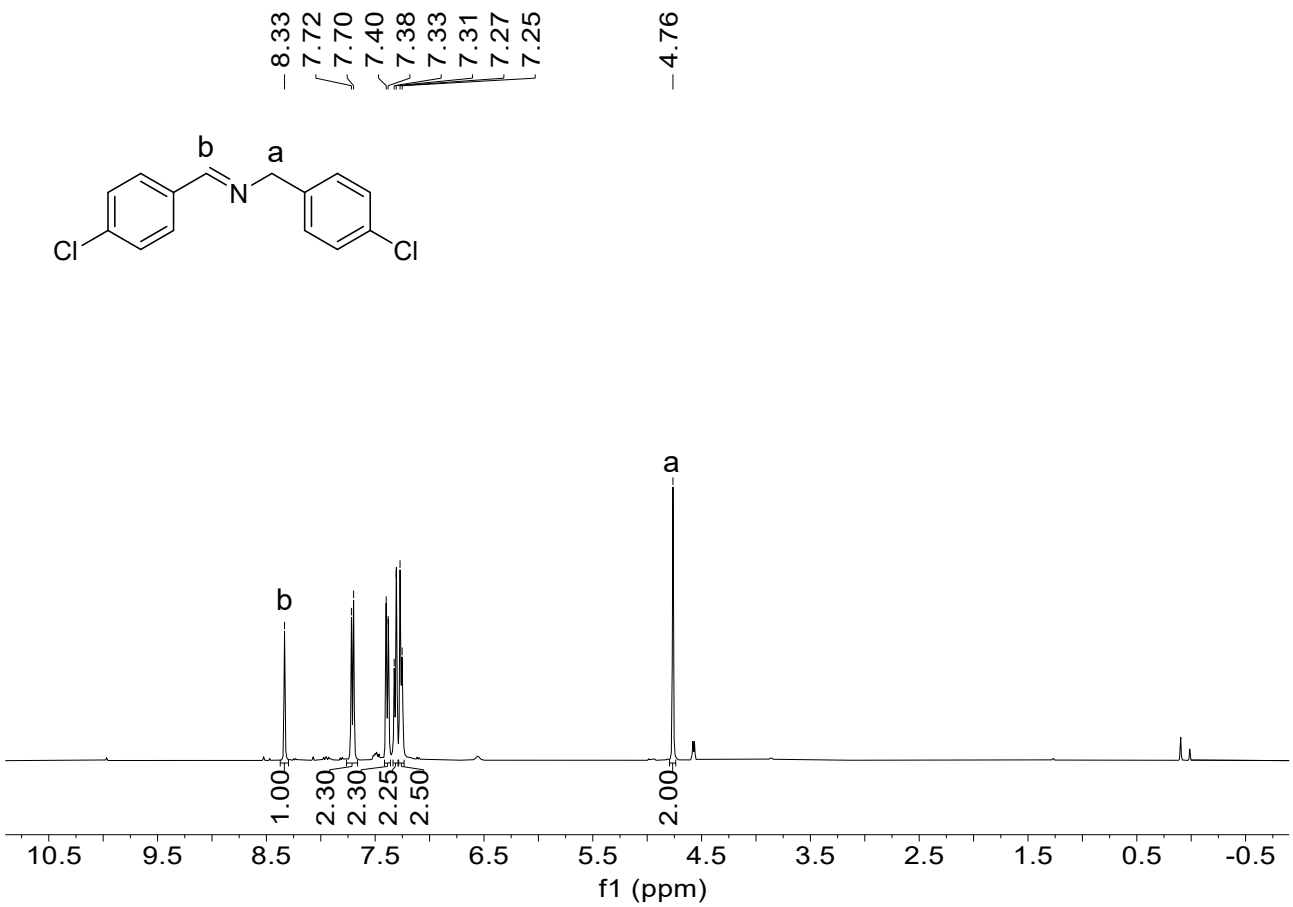

Fig. S20 ^{1}H NMR spectrum of *(E)*-N-(4-chlorobenzyl)-1-(4-chlorophenyl)methanimine (**2g**) (400 MHz, $CDCl_3$): δ=8.33 (s, 1H), 7.72~7.70 (d, 2H), 7.40~7.38 (d, 2H), 7.33~7.31 (d, 2H), 7.27~7.25 (d, 2H) and 4.76 ppm (s, 2H). Reaction conditions: blue LEDs (5 W), room temperature, in air, 10 h, conversion of 99%, selectivity of 99%.

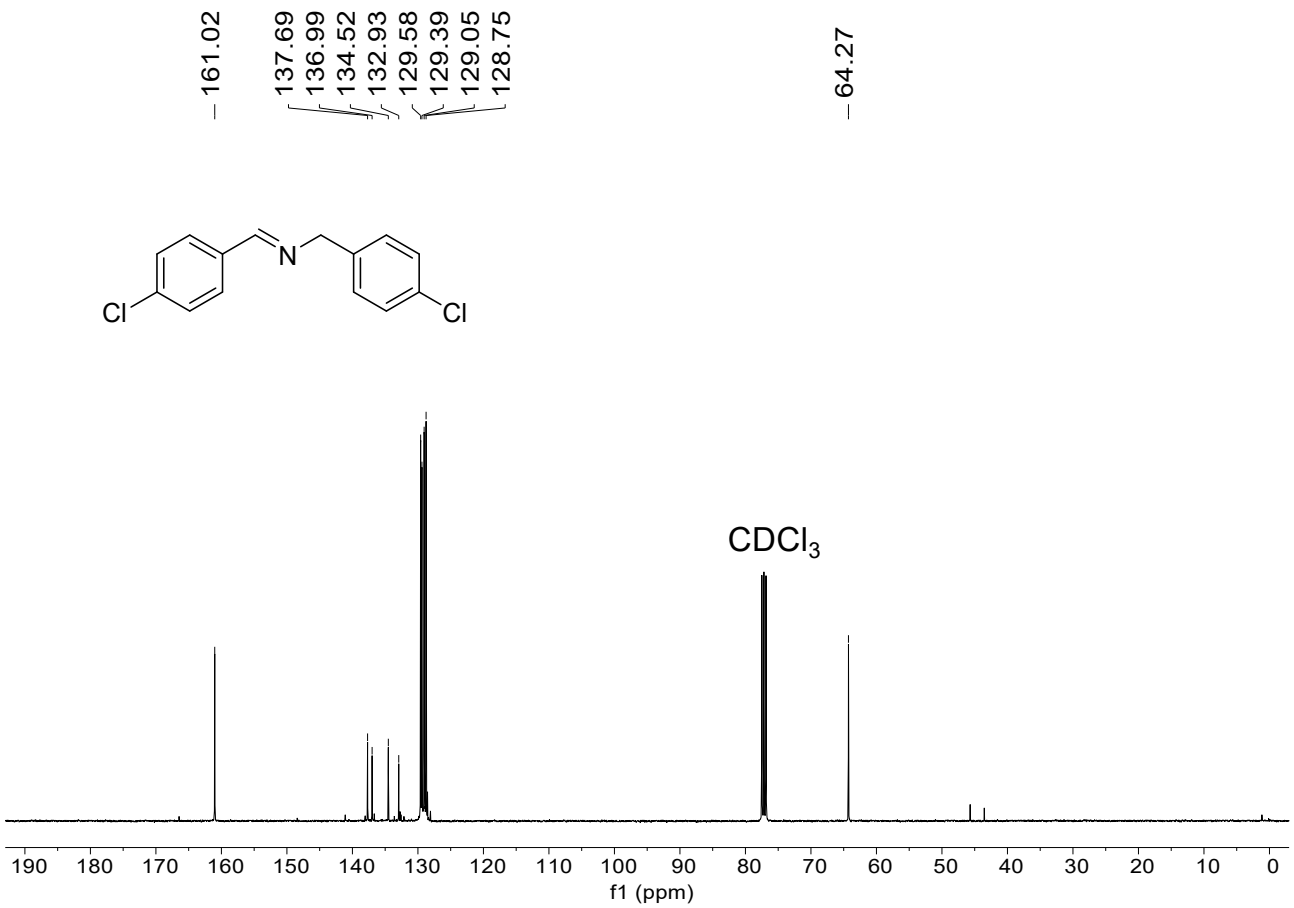

Fig. S21 ^{13}C NMR spectrum of *(E)*-N-(4-chlorobenzyl)-1-(4-chlorophenyl)methanimine (**2g**) (100 MHz, $CDCl_3$): δ=161.02, 137.69, 136.99, 134.52, 132.93, 129.58, 129.39, 129.05, 128.75 and 64.27 ppm.

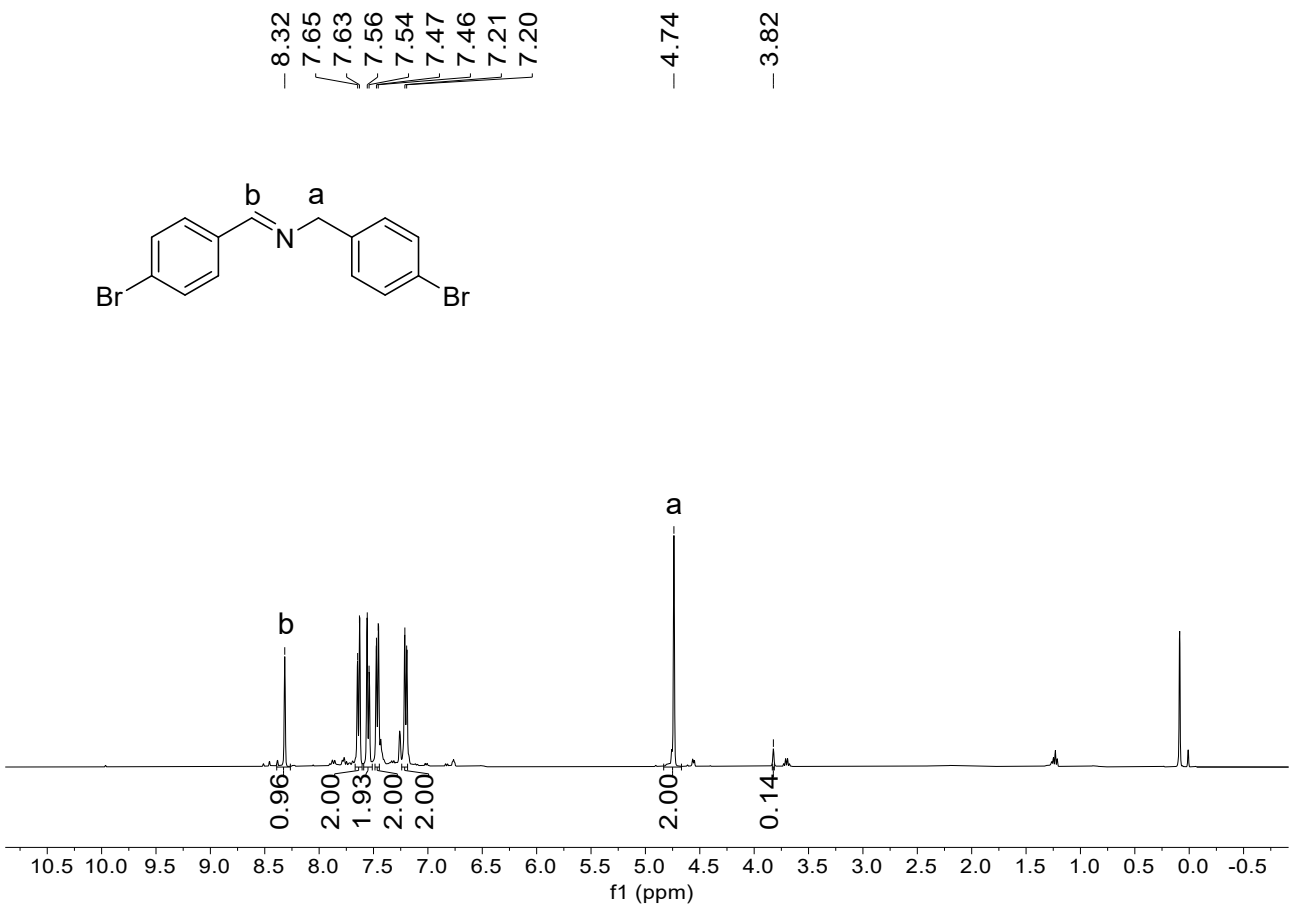

Fig. S22 ^{1}H NMR spectrum of *(E)*-N-(4-bromobenzyl)-1-(4-bromophenyl)methanimine (**2h**) (400 MHz, $CDCl_3$): δ=8.32 (s, 1H), 7.65~7.63 (d, 2H), 7.56~7.54 (d, 2H), 7.47~7.46 (d, 2H), 7.21~7.20 (d, 2H) and 4.74 ppm (s, 2H). Reaction conditions: blue LEDs (5 W), room temperature, in air, 10 h, conversion of 94%, selectivity of 99%.

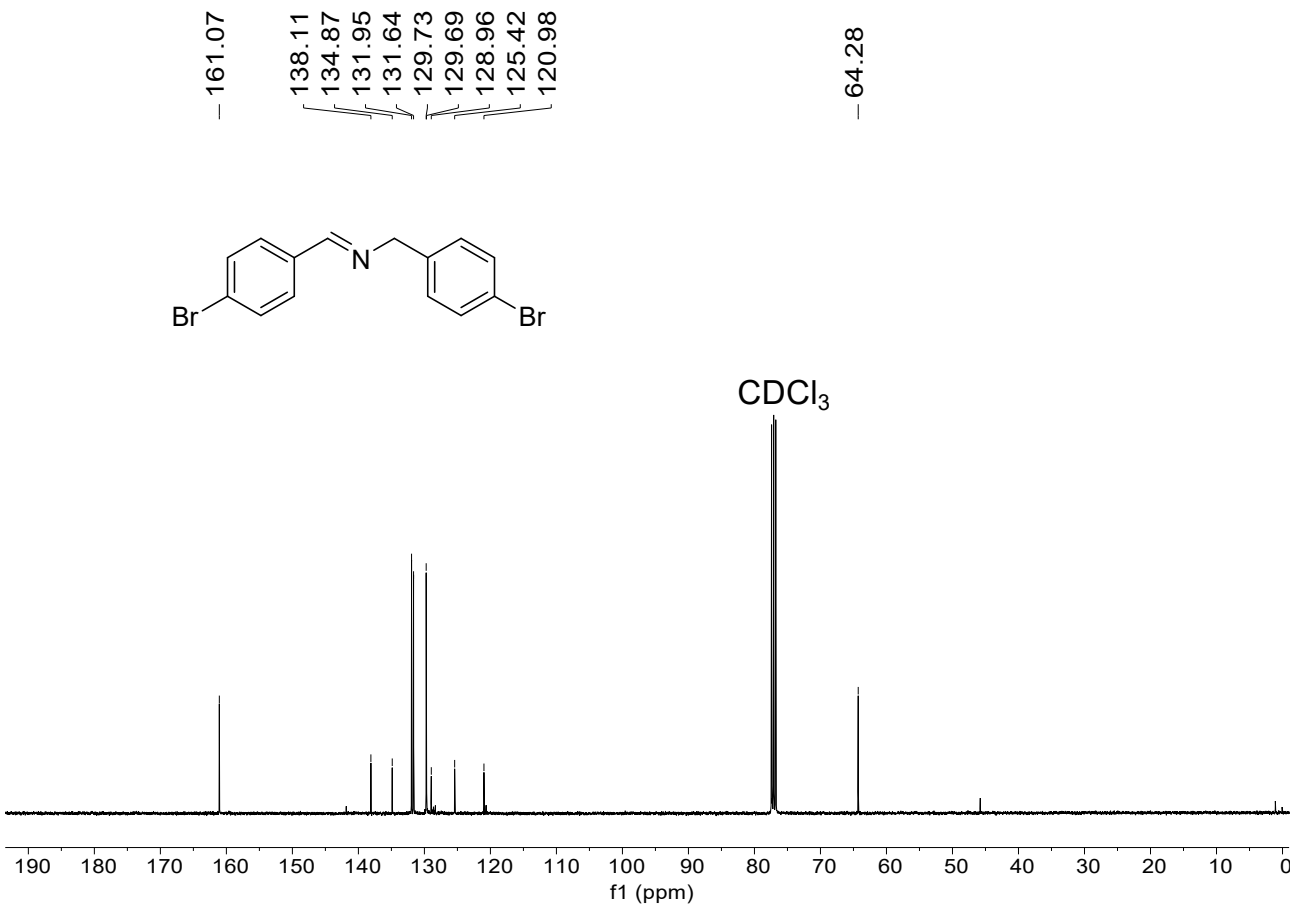

Fig. S23 ^{13}C NMR spectrum of *(E)*-N-(4-bromobenzyl)-1-(4-bromophenyl)methanimine (**2h**) (100 MHz, $CDCl_3$): δ=161.07, 138.11, 134.87, 131.95, 131.64, 129.73, 129.69, 128.96, 125.42, 120.98 and 64.28 ppm.

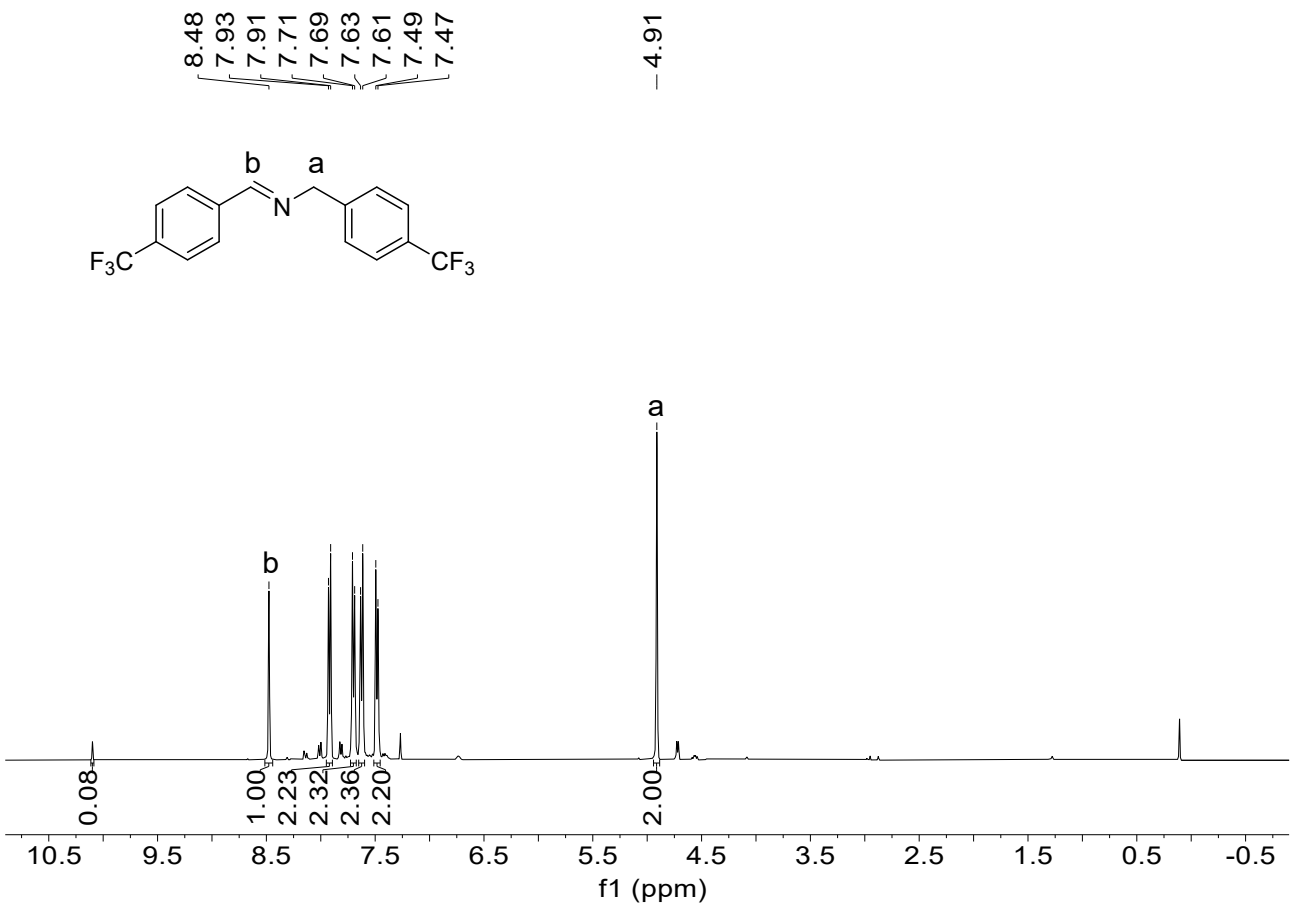

Fig. S24 ^{1}H NMR spectrum of *(E)*-N-(4-trifluoromethylbenzyl)-1-(4-trifluoromethylphenyl)methanimine (**2i**) (400 MHz, $CDCl_3$): δ=8.48 (s, 1H), 7.93~7.91 (d, 2H), 7.71~7.69 (d, 2H), 7.63~7.61 (d, 2H), 7.49~7.47 (d, 2H) and 4.91 ppm (s, 2H). Reaction conditions:blue LEDs (5 W), room temperature, in air, 10 h, conversion of 99%, selectivity of 97%.

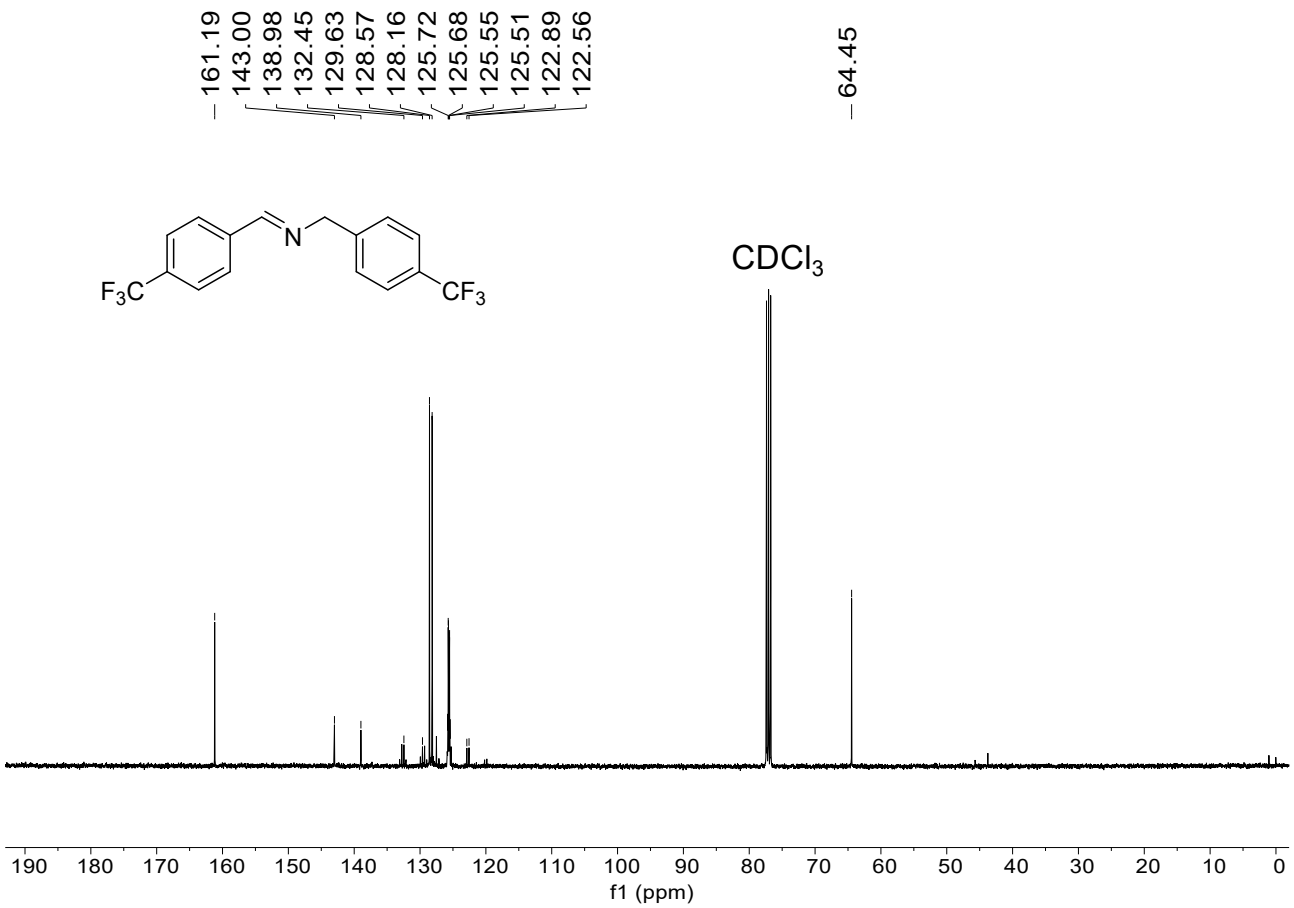

Fig. S25 ^{13}C NMR spectrum of *(E)*-N-(4-trifluoromethylbenzyl)-1-(4-trifluoromethylphenyl)methanimine (**2i**) (100 MHz, $CDCl_3$): δ=161.19, 143.00, 138.98, 132.45, 129.63, 128.57, 128.16, 125.72, 125.68, 125.55, 125.51, 122.89, 122.56 and 64.45 ppm.

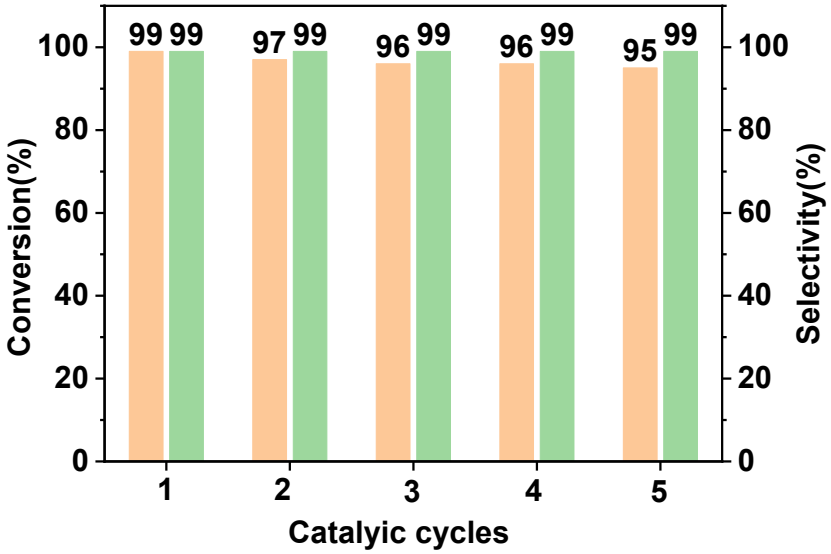

Fig. S26 Catalytic reusability of NA-POS-1 in the photocatalytic oxidative coupling of benzylamine. Reaction conditions: benzylamine (0.5 mmol), the catalyst NA-POS-1 (5 mg), blue LEDs (5 W), air atmosphere, room temperature, 6 h.

The adsorption experiment of the substrate benzylamine over the catalyst NA-POS-1

The amount of substrate benzylamine adsorbed by the catalyst NA-POS-1 was determined under dark conditions as follows: the substrate benzylamine (0.5 mmol, 53.6 mg) and the catalyst NA-POS-1 (5 mg) were magnetically stirred in dark at room temperature for 6 h under atmospheric air. Then, 3 mL ethyl acetate was added into a glass reaction tube and stirred for 12 h, then the solid catalyst NA-POS-1 was separated from the reaction mixture by the centrifugation. 50.4 mg benzylamine was obtained by concentrating under reduced pressure. Thus, the amount of substrate benzylamine adsorbed by the catalyst NA-POS-1 was about 6 wt%, which should be a normal adsorption amount in the catalytic reaction. The substrate benzylamine should be adsorbed by the catalyst NA-POS-1, which can make for enhancing the photocatalytic conversion of benzylamine to the product imine (*ACS Omega*, 2018, **3**, 12802).

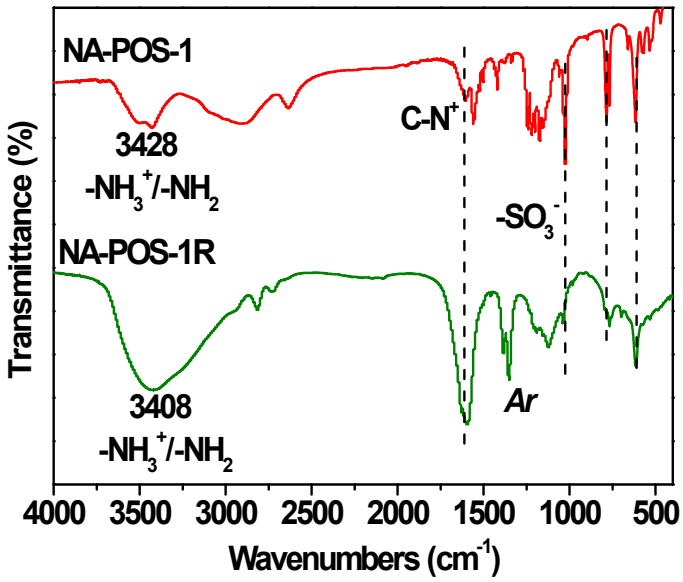

Fig. S27 FTIR spectra of the fresh catalyst NA-POS-1 and the recovered catalyst NA-POS-1R.

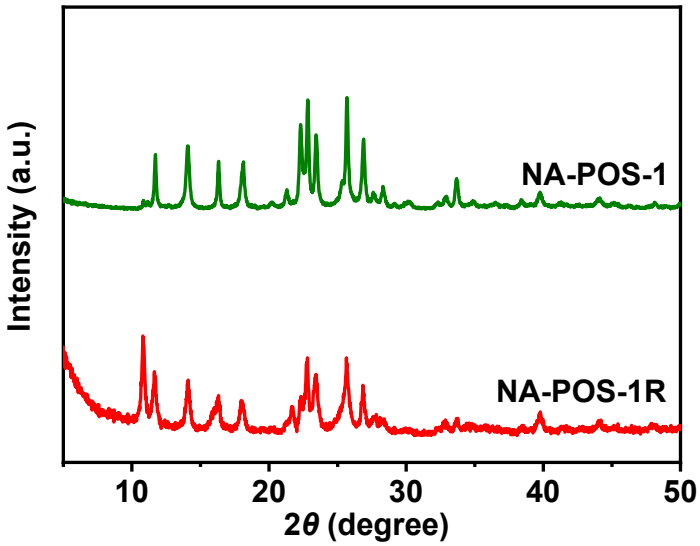

Fig. S28 XRD patterns of the fresh catalyst NA-POS-1 and recovered catalyst NA-POS-1R.

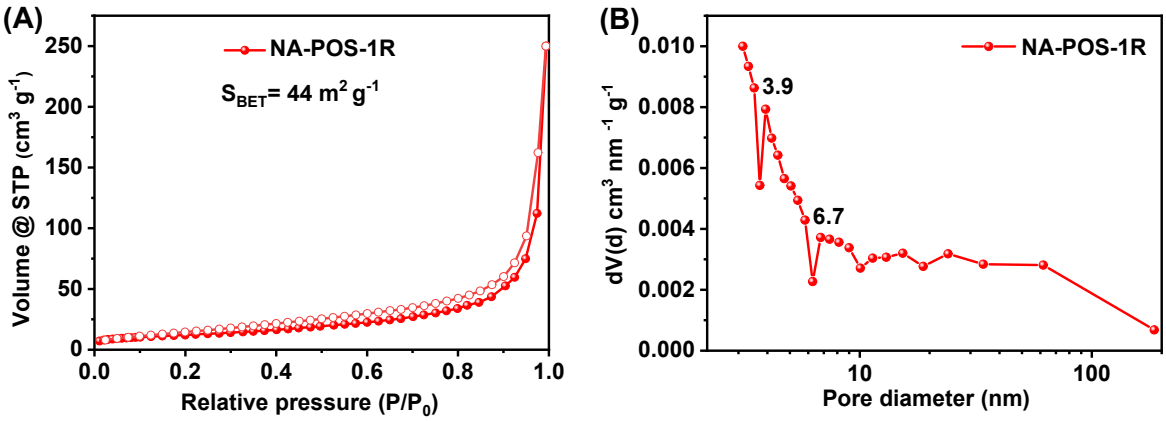

Fig. S29 (A) N_2 adsorption-desorption isotherms and (B) the BJH pore size distribution of the recovered catalysts NA-POS-1R.

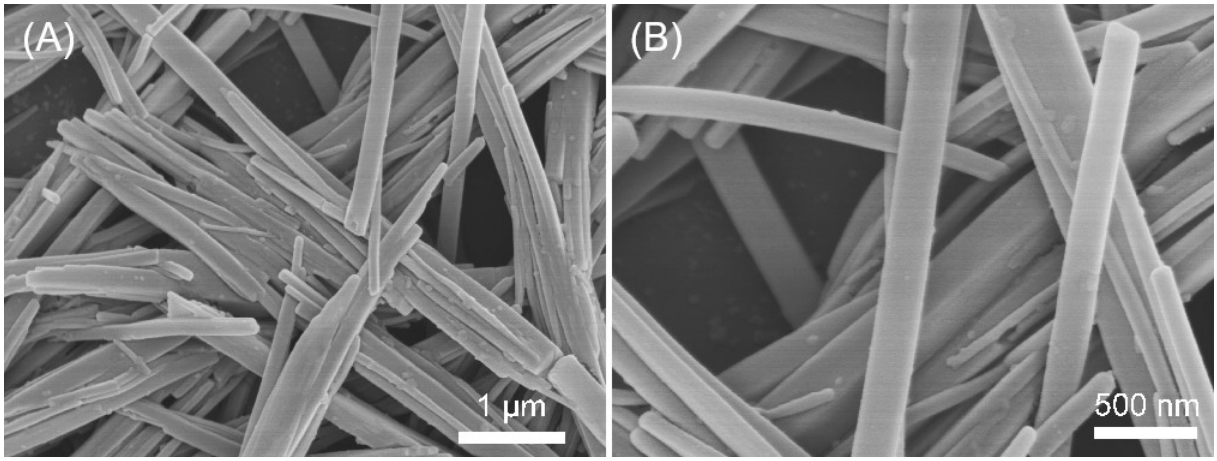

Fig. S30 The SEM images of the covered catalyst NA-POS-1R.

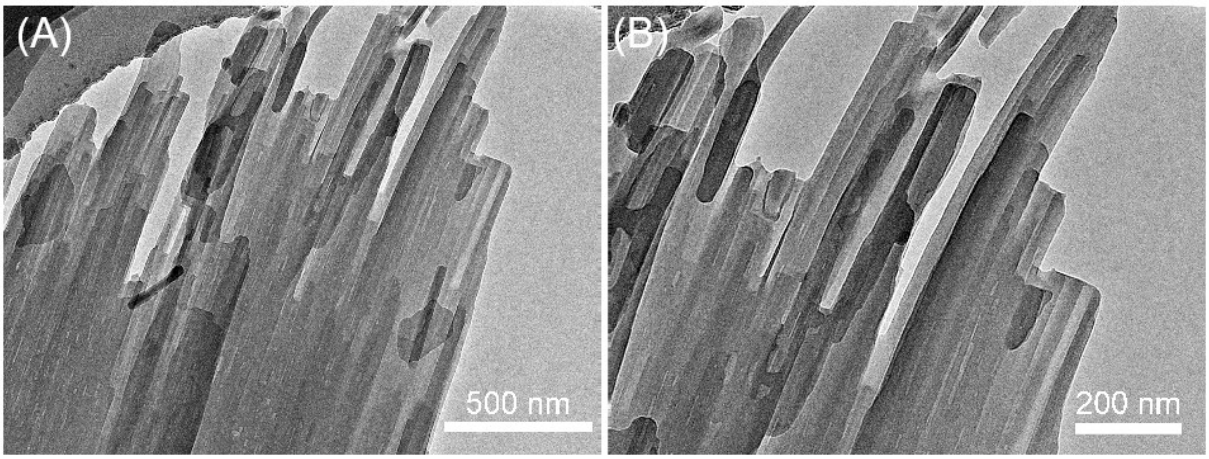

Fig. S31 TEM images of the covered catalyst NA-POS-1R.

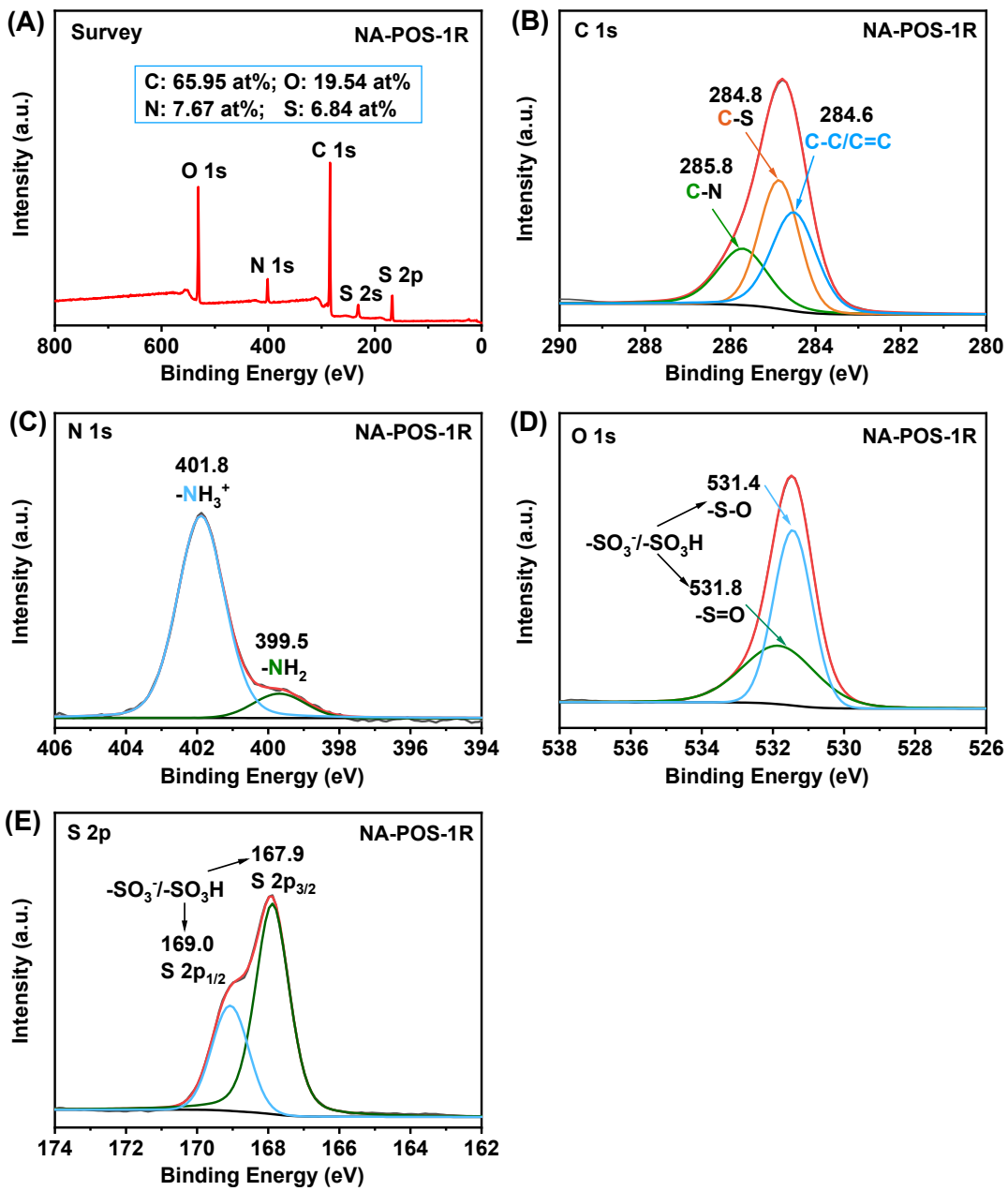

Fig. S32 XPS spectra of the recovered catalyst NA-POS-1R: (A) Survey: the elemental compositions with atomic concentrations of C (65.95 at %), O (19.54 at %), N (7.67 at %) and S (6.84 at %), (B) C 1s, (C) N 1s, (D) O 1s and (E) S 2p.

Table S5 Quenching experiments to assess the role of the key reactive oxygen species (ROS) over NA-POS-1.[a]

Entry	Scavengers	Role	Conversion (%) [b]	Selectivity (%) [b]
1	-	Standard conditions	99	99
2	*p*-BQ [c]	$O_2^{\bullet-}$ scavenger	19	99
3	NaN_3	$^1O_2$ scavenger	92	99
4	*t*-BuOH	•OH scavenger	94	99
5	$AgNO_3$	e^- trapper	7	99
6	KI	h^+ trapper	20	99

[a] Reaction conditions: benzylamine (0.5 mmol), NA-POS-1 (5 mg), scavengers (0.25 mmol), blue LEDs (5W), solvent-free, room temperature, in atmospheric air, 6 h. [b] The conversion and selectivity were determined by ^{1}H NMR analyses. [c] *p*-BQ (*p*-benzoquinone).

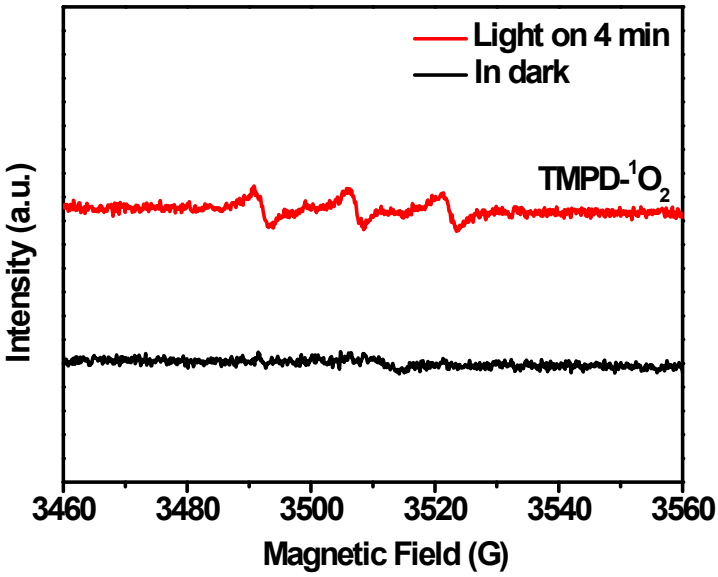

Fig. S33 EPR spectra of singlet oxygen ($^1O_2$) captured by 2,2,6,6-tetramethyl-4-piperidone (TMPD) upon blue light irradiation over the photocatalyst NA-POS-1.

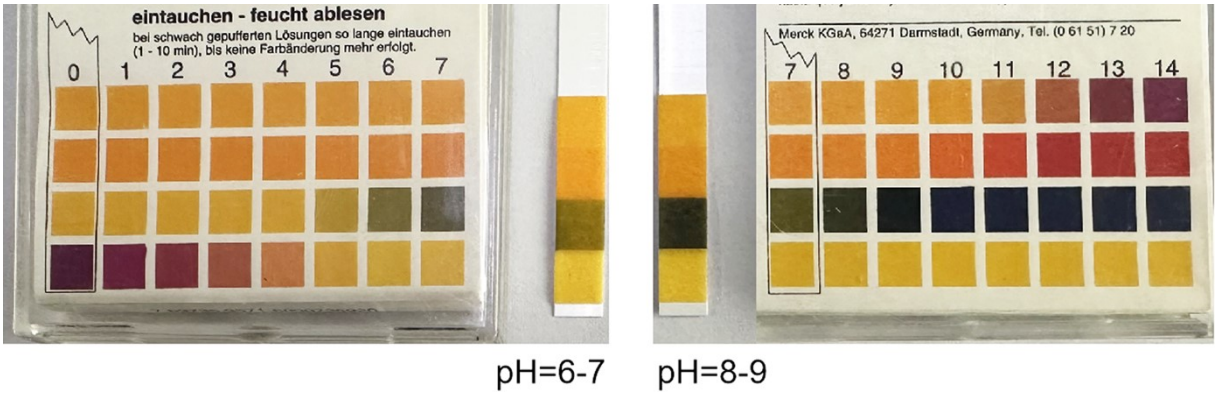

Fig. S34 The pH test for the by-product NH_3-containing aqueous solution after the reaction.

Determining the generation of ammonia (NH_3) in the photocatalytic oxidative coupling of benzylamine

Benzylamine (0.5 mmol) and the catalyst NA-POS-1 (5 mg) was mixed without any solvents, which was stirred and irradiated by blue LEDs for 6 h at room temperature in air. The releasing NH_3 gas during the reaction was continuously collected and passed into a test tube containing 2 mL distilled water, which subsequently was extracted by 5 mL dichloromethane for twice to rule out the possible influence of the organic substrate benzylamine and product imine. The aqueous layer was subject to pH test, showing its basic solution (pH=8-9, Fig. S34, right figure), indicating the generation of NH_3 during the reaction. After reaction, 2 mL distilled water was added to the solvent-free reaction system, and the solid catalyst NA-POS-1 sample was separated from the reaction mixture by high speed centrifugation. Then, the product imine and residual benzylamine in the homogeneous aqueous solution was extracted by 5 mL dichloromethane for twice. After subjecting to pH test, it could be found that the aqueous layer was neutral with pH=6-7 (Fig. S34, left figure), indicating the absence of NH_3 in the final reaction system. Therefore, we can conclude that NH_3 was produced in the photocatalytic oxidative coupling reaction of amines, and then the produced gas NH_3 was rapidly released from such a solvent-free photocatalytic system rather than accumulated in the catalytic system, which was different from previously reported organic solvent-involved photocatalytic reaction systems (see Table S4, such as *J. Mater. Chem. A*, 2023, **11**, 1208; *Sci. China Chem*., 2024, **67**, 1000). Therefore, the by-product NH_3 has no unfavorable effect for this photocatalytic reaction. On the contrary, the gaseous by-product NH_3 could be timely released from the present solvent-free catalytic system, which was beneficial to accelerate the catalytic reaction based on the chemical equilibrium theory. In our opinion, the useful by-product NH_3 can be recovered and recycled by the water absorption for subsequent multipurpose applications. We would in-depth study the photocatalytic oxidative coupling of benzylamines to imines coupled with NH_3 production in our future works.

Reference

S1 G. Xing, T. Yan, S. Das, T. Ben and S. Qiu*, Angew. Chem., Int. Ed.*, 2018, **57**, 5345.

S2 G. Xing, I. Bassanetti, S. Bracco, M. Negroni, C. Bezuidenhout, T. Ben, P. Sozzani and A. Comotti, *Chem. Sci.*, 2019, **10**, 730.

S3 S. Zhang, J. Fu, S. Das. K. Ye, W. Zhu and T. Ben, *Angew. Chem., Int. Ed.,* 2022, **61**, e202208660.

S4 A. Yamamoto, T. Hirukawa, I. Hisaki, M. Miyata and N. Tohnai, *Tetrahedron Lett.*, 2013, **54**, 1268.

S5 A. Comotti, S. Bracco, A. Yamamoto, M. Beretta, T. Hirukawa, N. Tohnai, M. Miyata and P. Sozzani, *J. Am. Chem. Soc.*, 2014, **136**, 618.

S6 A. Karmakar, R. Illathvalappil, B. Anothumakkool, A. Sen, P. Samanta, A. V. Desai, S. Kurungot and S. K. Ghosh, *Angew. Chem., Int. Ed.*, 2016, **55**, 10667.

S7 T. Ami, K. Oka, K. Tsuchiya and N. Tohnai, *Angew. Chem., Int. Ed.*, 2022, **61**, e202202597.

S8 A. Gak, S. Kuznetsova, Y. Nelyubina, A. A. Korlyukov, H. Li, M. North, V. Zhereb, V. Riazanov, A. S. Peregudov, E. Khakina, N. Lobanov, V. N. Khrustalev and Y. N. Belokon, *Cryst. Growth Des.*, 2021, **21**, 6364.

S9 Z. J. Wang, S. Ghasimi, K. Landfester and K. Zhang, *Adv. Mater.*, 2015, **27**, 6265.

S10 L. Liu, W.-D. Qu, K.-X. Dong, Y. Qi, W.-T. Gong, G.-L. Ning and J.-N. Cui, *Chem. Commun.*, 2021, **57**, 3339.

S11 J. Zhao, M. Xie, X, Chen, J.-K. Jin, W Zhao, J. Luo, G.-H. Ning, J. Liu and D. Li, *Chem. Asian J.*, 2023, **18,** e202300328.

S12 J. Jiang, X. Liu and R. Luo, *Catal. Lett.*, 2021, **151**, 3145.

S13 K. Wu, X.-Y. Liu, M. Xie, P.-W. Chen, J. Zheng, W. Lu and D. Li, *Appl. Catal. B: Environ.,* 2023, **334**, 122847.

S14 Z. Xu, K. Liu, S. Wang, Y. Chang, J. Chen, S. Wang, C. Meng, Z. Long, Z. Qin and G. Chen, *ACS Appl. Polym. Mater*., 2024, **6**, 701.

S15 C. Su, R. Tandiana, B. Tian, A. Tandiana, W. Tang, J. Su and K. P. Loh, *ACS Catal*., 2016, **6**, 3594.

S16 X. Liu, R. Qi, S. Li, W. Liu, Y. Yu, J. Wang, S. Wu, K. Ding and Y. Yu, *J. Am. Chem. Soc*., 2022, **144**, 23396.

S17 W. Wang, W. Gao, X. Nie, W. Liu, X. Cheng, N. Shang, S. Gao and C. Wang, *J. Colloid Interf. Sci.*, 2022, **616**, 1.

S18 F. Zhang, X. Dong, Y. Wang and X. Lang, *Small*, 2023, **19**, 2302456.

S19 Q. Wu, Z. Liu, Q. Su, P. Ju, X. Li, G. Li and B. Yang, *Chem. Commun*., 2020, **56**, 766.

S20 S. Liu, Q. Su, W. Qi, K. Luo, X. Sun, H. Ren and Q. Wu, *Catal. Sci. Technol*., 2022, **12**, 2837.

S21 Y. Liu, X. Jiang, L. Chen, Y. Cui, Q.-Y. Li, X. Zhao, X. Han, Y.-C. Zheng and X.-J. Wang, *J. Mater. Chem. A*, 2023, **11**, 1208.

S22 J. Jiang, X. Liu and R. Luo, *Catal. Lett*., 2021, **151**, 3145.

S23 N. Saini, N. Sharma, D. K. Chauhan, R. Khurana, M. E. Ali and K. Kailasam, *J. Mater. Chem. A*, 2023, **11**, 25743.